


Review

Overcoming Challenges in OLED Technology for Lighting Solutions

Rosalba Liguori ^{1,*} , Fiorita Nunziata ^{1,2}, Salvatore Aprano ³ and Maria Grazia Maglione ³¹ Department of Industrial Engineering, University of Salerno, 84084 Fisciano, SA, Italy² MATERIAS s.r.l., 80146 Napoli, NA, Italy³ Laboratory of Nanomaterials and Devices, ENEA Research Center, 80055 Portici, NA, Italy

* Correspondence: rliguori@unisa.it

Abstract: In academic research, OLEDs have exhibited rapid evolution thanks to the development of innovative materials, new device architectures, and optimized fabrication methods, achieving high performance in recent years. The numerous advantages that increasingly distinguish them from traditional light sources, such as a large and customizable emission area, color tunability, flexibility, and transparency, have positioned them as a promising candidate for various applications in the lighting market, including the residential, automotive, industrial, and agricultural sectors. However, despite these promising attributes, the widespread industrial production of OLEDs encounters significant challenges. Key considerations center around efficiency and lifetime. In the present review, after introducing the theoretical basis of OLEDs and summarizing the main performance developments in the industrial field, three crucial aspects enabling OLEDs to establish a competitive advantage in terms of performance and versatility are critically discussed: the quality and stability of the emitted light, with a specific focus on white light and its tunability; the transparency of both electrodes for the development of fully transparent and integrable devices; and the uniformity of emission over a large area.

Keywords: large area; lighting applications; OLED; transparent electrode; white OLED



Citation: Liguori, R.; Nunziata, F.; Aprano, S.; Maglione, M.G.

Overcoming Challenges in OLED Technology for Lighting Solutions. *Electronics* **2024**, *13*, 1299. <https://doi.org/10.3390/electronics13071299>

Academic Editors: Elias Stathatos and Spyros N. Yannopoulos

Received: 20 February 2024

Revised: 25 March 2024

Accepted: 27 March 2024

Published: 30 March 2024



Copyright: © 2024 by the authors. Licensee MDPI, Basel, Switzerland. This article is an open access article distributed under the terms and conditions of the Creative Commons Attribution (CC BY) license (<https://creativecommons.org/licenses/by/4.0/>).

1. Introduction

Currently, light emitting diode (LED) technology dominates the lighting industry, largely due to the numerous initiatives aimed at replacing outdated lighting systems reliant on incandescent bulbs. This transition is driven by the demand for enhanced energy efficiency, which, in solid-state lighting technology, is up to ten times greater thanks to the direct energy conversion phenomenon of electroluminescence and rapid switching. LED technology offers high-quality illumination, providing the flexibility to adjust the luminous flux, compact dimensions, and economic advantages, including an extended life cycle [1].

Meanwhile, significant advancements in the field of organic materials have paved the way for the introduction of a new lighting technology: organic light emitting diodes (OLEDs) [2,3]. Following initial research focused on improving the reliability of materials, monochromatic devices were first developed. After about a decade, the first white OLEDs were created, initially based on small molecules [4] in 1994 and later on polymers [5].

OLEDs are under active development as a prospective solid-state lighting technology [6–9]. They have attracted considerable attention in research over the past several decades, resulting in notable advancements, also thanks to support from initiatives within the industrial sector. Recent achievements in terms of efficiency and lifetime have favored the initial stages of commercialization, shifting the focus to aspects such as the production cost, yield, and exploration of aesthetic features, which emphasize their uniqueness compared to their inorganic counterparts [10,11]. Indeed, OLEDs can be designed as thin panels that, thanks to their flexibility and slim profile, can be integrated in various applications,

such as seamless luminaires, architectural building materials, and furniture, contributing to enhancing the functional but also the aesthetic aspects of spaces (Figure 1) [12,13].

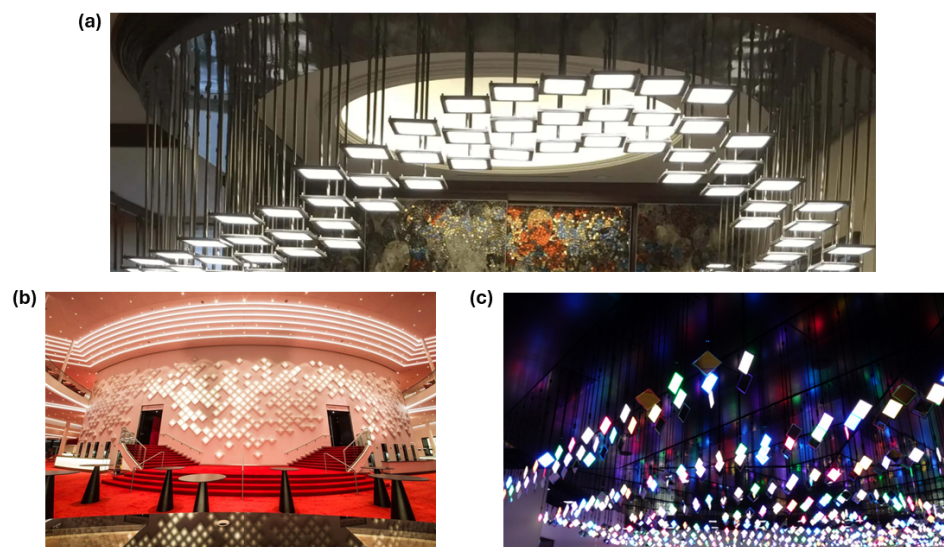


Figure 1. Examples of recent installations of OLED illuminaries. (a) OLED chandeliers composed of 226 Brite 2 FL300 nw OLED lighting panels, installed in New York in the reception area of a dentist’s office. Reproduced with the permission of [12]. (b) Dynamic OLED light installation designed by Hugo Timmermanns, which consists of 500 Brite FL300 OLED panels by Lumiblade, built into lamps in the shape of a pyramid. It creates light patterns that aim to attract visitors at the Theater an der Elbe (Hamburg, Germany), with variations on the theme of light in darkness. Reproduced with the permission of [13]. (c) Sumitomo colored polymeric OLED lighting panel installation. Reproduced with the permission of [13].

The uniqueness of OLEDs in emitting light directly from a surface, which can be quite extensive, as opposed to other lighting sources that are point-like, results not only in the potential for the complete customization of shapes [14] but also in the ability to operate at a reduced light intensity to achieve the same luminous flux. This feature minimizes heat generation, making OLEDs highly efficient. As for the characteristics of light, OLEDs emit a softly diffused light that replicates natural daylight, resembling the warmth of traditional incandescent lamps and contributing to creating a visually comfortable ambiance, with the additional benefit of energy efficiency [15,16]. The panels can also be transparent when turned off and offer the capacity for color tunability [17,18]. In addition, the fabrication techniques are compatible with flexible substrates requiring low temperatures; besides glass or metal substrates, OLEDs can be deposited on thin plastic sheets, ceramics, and fabrics, adding a further innovative aspect of versatility [19–21]. These qualities position them as a promising option for diverse applications in the lighting market, spanning the residential, industrial, automotive, and agriculture sectors, especially in scenarios where design innovation, energy efficiency, transparency, and reduced heat generation are crucial requirements.

An OLED device consists of a multilayer structure (Figure 2) [22–24], traditionally emitting through a substrate (bottom-emitting OLED), primarily composed of an emissive layer (EML) sandwiched between a transparent anode (commonly based on indium tin oxide, ITO), deposited on a transparent substrate, and an opaque metal cathode. In the emissive layer, the injected charges, electrons, and holes meet to form excitons, which are excited molecule states. A top-emitting device has the same structure but with a transparent top electrode, and the substrate can also be opaque. The third possible configuration, particularly interesting for lighting applications, is that of a transparent OLED (TrOLED), where emission occurs through both electrodes, which must therefore be transparent. These

can be integrated into transparent surfaces, such as windows and glass walls, adding new functionalities to lighting [25].

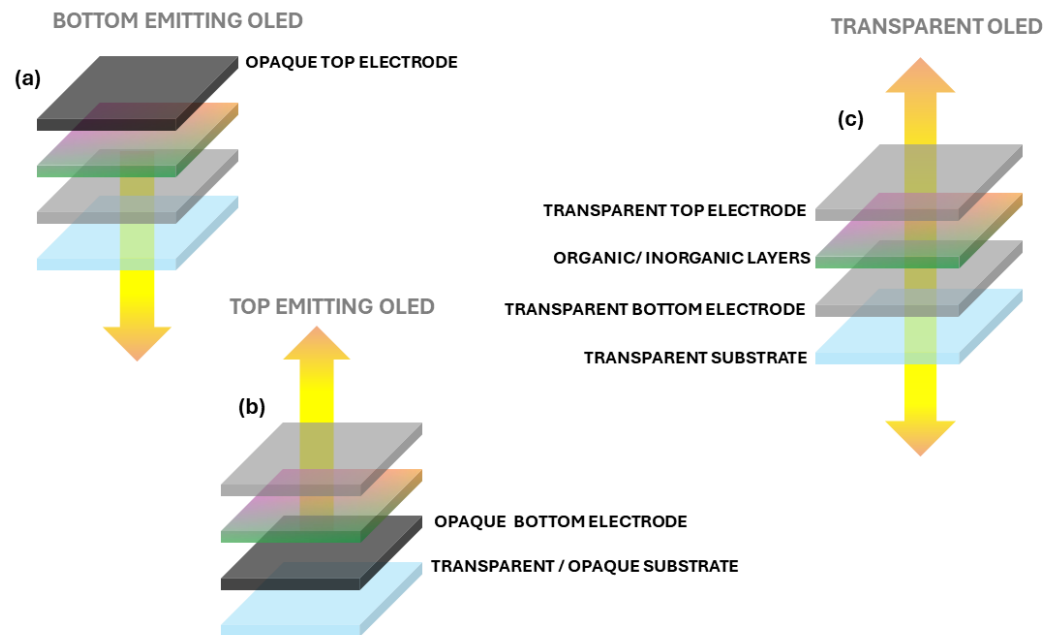


Figure 2. Structure of a (a) bottom-emitting OLED device, (b) top-emitting OLED device, and (c) transparent OLED device, emitting from both sides.

The light is generated by the recombination in the emissive layer of electrons and holes; therefore, an OLED can be designed to emit any color by carefully choosing the materials forming the emissive layers, including white with various color temperatures. The OLED structure has been gradually made more complex to enhance its efficiency, with the addition of layers serving specific functions (Figure 3): between the anode and EML, a hole injection layer (HIL), a hole transport layer (HTL), and an electron blocking layer (EBL) can be inserted, while, between the cathode and EML, an electron injection layer (EIL), an electron transport layer (ETL), and a hole blocking layer (HBL) can be included. While the injection and transport layers improve the injection from the contacts and the transport of charges to the emissive layer, the blocking layers prevent the loss of charges in the opposite direction and confine the excitons. All layers are ultimately protected from the environment by a cover, due to the high sensitivity of many of the materials used to moisture and oxygen [26], which can reduce the lifespan of the panels [27,28]. The cover is sealed to the substrate using an epoxy adhesive, and, often, a desiccant is included inside to capture moisture and oxygen that may permeate the panel over time through the sealant (Figure 3) [29].

Certainly, compared to a traditional glass substrate, a plastic substrate is more susceptible to moisture permeability issues and requires the introduction of alternative solutions. Among these, a recent trend is to use thin and flexible glass substrates [30]. Equally important is the light extraction layer, which significantly contributes to the total efficiency [31,32].

OLED panels also require driver circuits that convert the line voltage into a DC current. These driver circuits can also impact the final product efficiency. A constant-voltage driving circuit is not advisable, as it would allow the current to change based on various external parameters and reduce the panel's lifespan. Alternatively, it is desirable to have a driver circuit that allows for light dimming by adjusting the driving current and is capable of adjusting the driving voltage to compensate for the reduction in current over time [33,34].

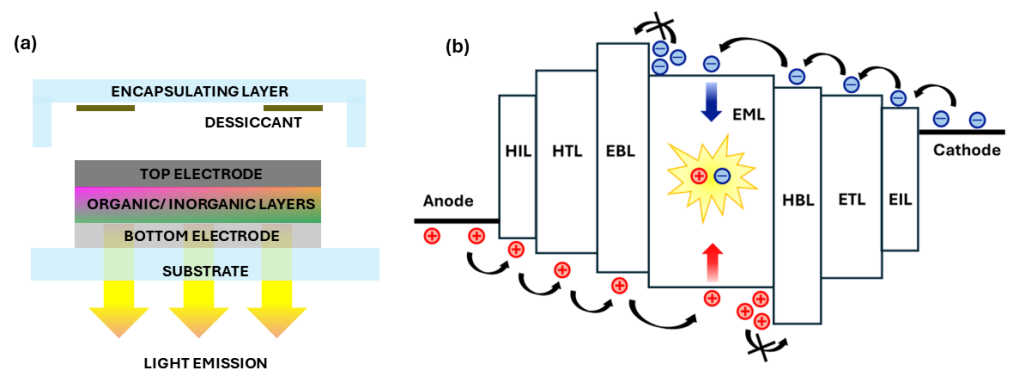


Figure 3. (a) Schematic cross-section of an encapsulated bottom-emitting OLED. (b) Energy diagram of a typical multilayer OLED, highlighting the functions of all possible layers: generally, not all are present as multiple functions are combined in a single layer.

OLEDs, to be employed in lighting applications, must meet specific requirements, such as high brightness, high efficiency, low costs, low power consumption, and a long lifetime [35]. The performance of an OLED device is typically evaluated based on three types of efficiency [23]: the external quantum efficiency (η_{EQE}), the current efficiency (η_c), and the luminous efficacy (η_L), often referred to as the power efficiency or lighting efficiency [36]. The first figure of merit, the external quantum efficiency (%), describes the number of outcoupled photons per injected charge and includes the charge balance, singlet-triplet factor, radiative quantum efficiency, and light coupling efficiency. The current efficiency (cd/A) and luminous efficacy (lm/W) are photometric parameters that consider the sensitivity of the human eye. The current efficiency is calculated from the luminance and is defined as the ratio between the luminance obtained in the forward direction and the current density passing through the device. The luminous efficacy is defined by the ratio of the luminous flux to the electrical power.

In addition to those described above, OLED manufacturers need to optimize other two parameters: the luminance and lifetime. The luminance (cd/m^2) determines the brightness of the light emitted. The lifetime of OLEDs is an important indicator in evaluating the stability of these devices, and a longer device lifetime is vital for their successful commercial use [37]. The intrinsic qualities of the materials and device architectures mostly influence the operational lifetime, which can be quantified in terms of the lumen maintenance life L_p (hours), which is defined as the elapsed operating time over which the light source will maintain a percentage p of its initial light output: the 50% lumen maintenance value (L50) is used for lighting and display purposes, while L70 (70% lumen maintenance) is required for architectural lighting [22]. Table 1 shows a comparison of the luminous efficacy and lifetime values of OLEDs, with corresponding metrics for other lighting technologies.

Table 1. Comparison of OLED lighting's luminous efficacy and lifetime with those of other commercially available lamps [38–40].

	OLED	LED	Fluorescent Lamp	Incandescent Lamp
Luminous Efficacy [lm/W]	50–100	60–160	60–80	15–20
Lifetime [h]	5000–10,000	50,000–100,000	7000–15,000	700–2000

The characteristics of light can be indicated through three parameters: the Commission Internationale de L'Eclairage (CIE) coordinates, the color rendering index (CRI), and the correlated color temperature (CCT) [41]. For lighting applications, to ensure color purity, the light should have CIE coordinates close to the ideal white point, which is (0.33, 0.33), but they can fall within a much broader range. The CRI, namely the ability to reproduce

the color of the illuminated object, ranges from 0 to 100, but it must be greater than 80 for lighting applications. It is excellent in OLEDs and is one of the aspects that make them interesting not only for indoor illumination but also in professional video and photographic applications. This is because organic materials inherently have a broad luminescence spectrum, and by opportunely combining materials with different emission colors, it is possible to achieve an extension across the entire visible spectrum. Finally, there is the CCT, which, in the case of white light for illumination, takes values ranging from 2500 K (warm light) to 6500 K (cool light).

Currently, OLEDs are primarily used for indoor architectural applications due to their sensitivity to moisture and air, although proposals have been presented in the automotive sector [42]. Current projects involve the combination of LEDs and OLEDs in lighting systems, where the former generates directional light while the latter diffuses it. OLEDs are utilized in wall coverings such as ceramic tiles, with the addition of digital control to create changing effects in brightness or decoration. They are also employed in very large ceiling panels or as backlighting for shelves and niches. Additionally, OLEDs find use as signaling lights for aircraft cabins, exit paths in buildings, decorative signage for company logos, and similar purposes [10].

2. OLED Lighting Market: Evolving Trends and Current Hurdles

While, in the field of academic research, tremendous advancements have been made in terms of luminous efficacy, one of the key factors for lighting applications, reaching values as high as 160 lm/W in recent years [43], in the industry, field OLEDs have to compete with their inorganic counterparts. Certainly, they are competitive regarding the ability to obtain large-area and flexible panels with a customizable design and tunable chromaticity in a wide range, but further efforts are needed to narrow the gap in terms of efficiency. The first meaningful results in terms of area and efficiency were achieved by GE Global Research, which, in 2004, fabricated a 2 ft × 2 ft white OLED panel with a CCT of 4400 K, a CRI of 88, and efficacy of 15 lm/W [44]. In 2008, Osram researchers demonstrated the possibility of improving two crucial characteristics simultaneously, namely the efficacy and lifetime, reaching 46 lm/W with a CIE of (0.46, 0.42) and 5000 h, respectively, with a prototype of almost 100 cm², at a brightness of 1000 cd/m² and a CRI of 80 [22]. The following year, a dimmable round panel generating a warm white color (2800 K), emitting no UV or IR radiation, was released with the name ORBEOS (Figure 4a) [45]. It was the result of rapid advancements reached in the context of the project OPAL 2008, which had the aim of developing an OLED production technology capable of achieving the cost target of a few Euro cents per cm² for a high performance white OLED device. The project, using organic vapor phase deposition (OVPD) technology, involved other companies, including Philips, which, in 2011, in collaboration with Konica Minolta, started to produce warm white panels (Lumiblade) with luminous efficacy of 45 lm/W, a lifetime of 10,000 h, and luminance of 1000 cd/m² [46].

In 2010, Panasonic demonstrated the ability to extend the OLED panel lifetime to over 80,000 h by using an efficient heat radiation structure in order to prevent thermal breakdown and by improving the encapsulation structure with an inorganic/organic passivation layer, thus obtaining a 8 × 8 cm² panel uniformly operated at 5000 cd/m² and with a CRI of 94 [47]. Subsequent mass production involved a color-tunable OLED lighting panel by Verbatim, called VELVE, with an area of 14 × 14 cm², exhibiting typical efficacy of 28 lm/W (Figure 4b) [13]. Based on small molecule emitters and partially using solution deposition techniques, they offered the possibility of tuning the CCT between 2700 and 6500 K and the color [48]. In the same year, the Universal Display Corporation developed white OLED (WOLED) panels with an area of 15 × 15 cm², CCT of 2790 K, and CRI of 86, reaching efficacy of 58 lm/W [49].

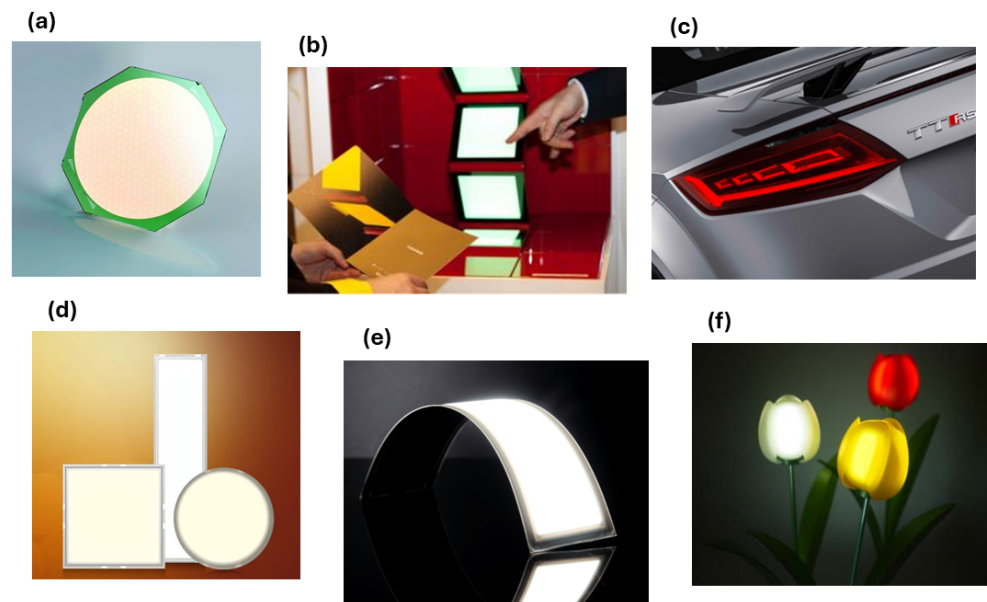


Figure 4. Evolution of OLED production for lighting applications. (a) Osram ORBEOS OLED panel [45]. (b) Verbatim VELVE. Reproduced with the permission of [13]. (c) OLED rear lights covering an Audi car. Reproduced with the permission of [13]. (d) Lumiblade Brite3 by OledWorks. Reproduced with the permission of [12]. (e) Lumicurve Wave by OledWorks. Reproduced with the permission of [12]. (f) Konica Minolta OLED Tulip illumination demonstrated in Japanese theme park with shining flexible OLED petals. Reproduced with the permission of [50]. Copyright 2017, John Wiley & Sons Books.

Within a few years, almost all lighting companies have displayed OLED luminaires and made significant investments in the production of panels, introducing also polymer and hybrid technologies and flexible designs, extending even to the automotive sector. In 2013, Audi, Philips, and Merck presented their OLED lighting prototypes for car rear lights, utilizing also curved glass substrates and transparent contacts (Figure 4c) [13]. Efficacy of 100 lm/W and an expected lifetime of 40,000 h were meanwhile obtained by LG Chem by using the pixellation technique, which involves the subdivision of the light emitting area ($90\text{ mm} \times 90\text{ mm}$) into thousands of tiny pixels of less than 1 mm^2 , thus avoiding failure due to abrupt electrical shorting and meeting the requirements of general lighting sources [51]. Although the first prototypes of flexible panels appeared in 2010, it was in 2018 that the bending radius of an OLED lighting panel fabricated on a thin glass substrate by OledWorks (Figure 4e) was decreased to 10 cm, reaching 60 lm/W, while their rigid panels' efficacy increased from 40–60 lm/W (Brite1) to 80–90 lm/W in the advanced generation Brite3 (Figure 4d) [12,30].

The improvement in efficacy was also due to the optimization of the light extraction technique, as proposed by Pixelligent, which involved a solution-processable nanocomposite, creating an extraction structure with a refractive index proportional to the nanocrystal loading, enabling the realization of both high-refractive-index layers and an index gradient to direct light in a specific direction [52,53]. While WOLED panels undergo advancements in terms of technical performance and reliability, their broader adoption in the lighting market is increasingly exploiting the commercial and aesthetic opportunities that they provide. Thus, ultraflexible thin OLED films have appeared, with various 3D shapes, from globes to candle flames and flowers (Figure 4f) [11], or they can be integrated with paper packaging. The focuses of companies in recent years have been mostly automotive lighting and mass production through roll-to-roll techniques, obtaining bendable and durable OLED panels for plastic substrates used in general lighting and the architecture sector [46].

While, on one hand, OLEDs surpass the limitations of LED-based light sources, such as overheating and blue light content, other critical aspects need to be considered for widespread industrial deployment. Long-term reliability is fundamental for a light source, both concerning the electrical properties, such as the operating voltage and power, and the optical properties, such as the luminous efficacy and color quality (CCT and CRI). OLED degradation, which leads to a reduction in lifetime, occurs due to both extrinsic and intrinsic factors. Among the extrinsic elements are humidity and oxygen, whose effects are limited by encapsulation. Intrinsic mechanisms, on the other hand, are associated with electrical stress and include increased trap density, reduced mobility, and worsened charge injection. Many studies have investigated these phenomena [40,54–56] but also demonstrated that the long-term reliability is acceptable for general lighting applications according to the IEC 62922 standard (OLED panels for general lighting—Performance requirements) [57]. Based on the same analyses, it has emerged that improvements aimed at long-term reliability are required for panels with a larger area, which still exhibit faster color degradation, and for the control gears of luminaires whose design needs to better suit OLEDs' features.

In terms of the environmental impact associated with large-scale OLED production, OLEDs are often regarded as environmentally friendly for two primary reasons. Firstly, the fabrication of organic devices relies on low-temperature processes, necessitating minimal energy investments. Secondly, the majority of organic devices do not contain materials with substantial environmental or health implications. In fact, only a limited number of studies have thus far explored the potential environmental impact of OLEDs, with a particular emphasis on displays and on the presence of metals [58]. The findings of these studies reveal that OLED displays must be treated as hazardous waste during disposal due to their higher resource toxicity potential compared to LCDs, associated with the high concentrations of metals such as gold, arsenic, and cadmium. However, the main source of metal-based components is attributed to the OLED driver circuit, which contains a larger number of transistors, electrodes, and capacitors.

Conversely, despite the growing demand for short-lived or disposable devices, the industry has paid less attention to the necessity of making OLED technology more environmentally sustainable: there is a lack of focus on introducing new devices that facilitate the recycling of all components and the recovery of valuable materials through sustainable methods [59,60]. Meanwhile, scientists have made strides in the development of bio-compatible materials to realize various OLED layers. To this end, low-cost, lightweight, flexible, and recyclable cellulose has been used as a substrate and encapsulation layer [61,62]. Flexible carbon nanotubes and graphene, combined with conductive materials, as well as natural silk fibroin embedded with silver nanowires and human eumelanin integrated into PEDOT-PSS, have been successfully used to produce electrodes with good transparency and conductivity [19,63,64]. Furthermore, bio-composite blends of conjugated polymers with vitamins, nucleic acids, and proteins have enabled the production of water-soluble emissive or injection layers, reducing the extensive use of organic solvents [65–69].

Despite the involvement of several companies in OLEDs for lighting applications, production remains limited. The primary constraint continues to be the price, which remains too high for commonplace applications such as shelf lighting, under-cabinet illumination, offices, and classrooms [10]. Additionally, due to their low luminance for small surfaces, OLEDs are not suitable for tasks requiring focused lighting. However, they become more feasible when used for decorative and cutting-edge purposes. Currently, OLEDs also face challenges related to interchangeability among manufacturers, particularly concerning panels, connectors, and drivers. Consequently, contrary to the industry aspirations, the OLED market remains a niche market, mainly confined to custom decorative luminaires, automotives, and medical lighting, where OLEDs have the potential to differentiate themselves from LEDs. To achieve a significant reduction in costs, it is necessary to consider the factors driving the production expenses: presently, the primary cost driver among materials is the inorganic component present in the panel, including the current driver

and packaging. To these labor costs, the infrastructure investments and fixed costs are added. The production cost diminishes rapidly with an increase in production capacity [70]. Moreover, the growing competitiveness of OLEDs is driving the utilization of equipment and infrastructure originally designed for display manufacturing. Recently, there has been an increased focus on the high-speed fabrication of organic semiconductors on flexible substrates that are compatible with or integrated into roll-to-roll processing, resulting in a reduction in costs [71,72].

In conclusion, despite their promising characteristics, the widespread industrial production of OLEDs encounters notable challenges. Addressing these issues is essential to realize the full potential of this technology and allow its integration into different sectors. Among the challenges that OLED lighting must address to achieve performance comparable to that of competitive solutions, we analyze those related to managing the emission spectra, ensuring the transparency of contacts, and achieving homogeneous emission over large areas, and we explore potential solutions.

3. Challenges in Light Color

The emission of white light requires a combination of primary or complementary colors. Apart from solutions that involve stacked or pixel-designed individual OLEDs, which are structurally complex and inefficient, it is possible to achieve white light with a single device using individual emitters or multiple emitters that are properly combined [73].

The significant progress achieved in white OLED (WOLED) technology is primarily based on the efforts of chemists in developing new materials that ensure high performance and improve the lifetime while simultaneously maintaining simplicity and low costs in production [74–77]. The materials that can be used to fabricate white OLEDs are fluorescent, phosphorescent, and thermally activated delayed fluorescence (TADF) materials. As depicted in Figure 5, in conventional fluorescent materials, 75% of the excitons, which are in the triplet state, do not emit light, while only the 25% in the singlet state are radiative. Conversely, phosphorescent materials can theoretically achieve 100% efficiency by utilizing all types of excitons: the transition from the triplet state to ground state is radiative and the intersystem crossing (ISC) mechanism is facilitated by the use of metallorganic complexes, based on rare metals like iridium and platinum [78–80]. However, these metal elements, mostly expensive, precious, and toxic, pose a barrier to the development of phosphorescent OLEDs. On the other hand, TADF materials can exploit all excitons without resorting to noble metals but by relying on the reverse intersystem crossing (RISC), i.e., the thermally activated transition of triplet excitons to singlet, which produces delayed fluorescence [81,82]. This allows internal efficiency close to 100% to be achieved. However, RISC is made possible only in molecules carefully designed to reduce the energy gap between the excited singlet and triplet states.

The simplest way to obtain white light is to blend different lumiphores, such as the first attempt with red, green, and blue phosphors in a single matrix [4], using straightforward vacuum- or solution-based techniques. However, there are some drawbacks to consider, such as the phase separation leading to non-homogeneities and the energy transfer among different phosphors, generating color shifts in the emitted light. These issues are not easily controllable and can result in unstable and poor-quality emissions.

A solution to phase separation is to combine the various components of the blend, as occurs with copolymerization into a single copolymer of different chromophores covering the entire visible spectrum [83–85]. Polymeric OLEDs also provide the advantage of being easily manufacturable but require careful molecular design to ensure the uniform distribution of the chromophores within the film and to control the energy transfer between species. These requirements have led to the development of device architectures containing a stack of multiple layers, where each material has a specific functionality. However, it is necessary to ensure that the different contributions in various regions of the spectrum from each layer are balanced, considering that emission in a layer can occur both due to recombination within the layer itself and due to excitation resulting from energy transfer

from an adjacent layer. Therefore, careful design in terms of the arrangement, thickness, and energy levels of each layer is required. In such circumstances, layers with blocking functions play a fundamental role [86,87].

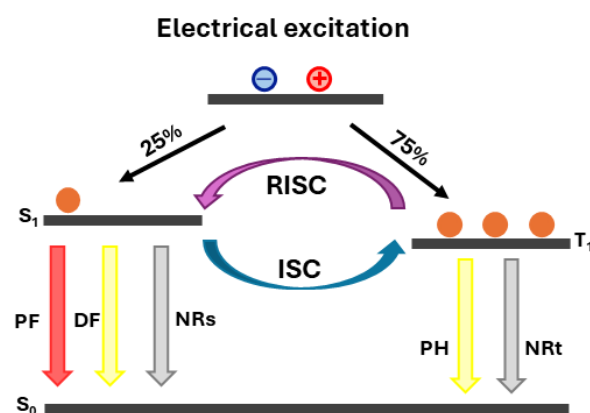


Figure 5. Transition processes of electrically generated excitons. S_0 : ground state, S_1 : singlet excited state, T_1 : triplet excited state, PF: prompt fluorescence, DF: delayed fluorescence, NRs: non-radiative singlets, PH: phosphorescence, NRt: non-radiative triplets.

WOLEDs based entirely on phosphorescent materials are affected by undesirable effects. One is the color shift problem caused by the instability of blue-emitting phosphors. Another is the efficiency roll-off induced by exciton quenching in the host matrix and transport layers and by triplet–triplet annihilation. An approach to reducing these issues involves dispersing phosphors as dopants with lower triplet energy in a blue fluorescent material with high triplet energy. In this way, a hybrid configuration is obtained, providing higher stability and performance [88,89]. The issues that can be encountered in these OLEDs are that the energy level of the triplet is not sufficiently high and the poor photoluminescence yield of the blue fluorophore. In such a case, the reverse energy transfer of triplet excitons from phosphors to the blue fluorophore would be established, which, being non-radiative, would reduce the efficiency. An advanced layer design can maximize the efficiency of such devices: the idea is to drive the excitons formed in the singlet state towards the blue fluorescent layer and transfer the triplet excitons to green, orange, or red phosphorescent emitters, with the aim of achieving internal efficiency close to 100% [90–93].

A further method to obtain white light is color down-conversion: it employs the combination of a blue OLED with a color conversion layer (CCL), typically composed of a host layer doped with an organic or inorganic dye. The blue emitter, which is electrically excited, optically excites the CCL, generating a complementary color [94,95]. However, this structure is quite challenging to obtain due to the low stability and efficiency of the blue emitter and the difficulty in obtaining materials that enable efficient color conversion.

We have investigated the relationship between the microstructure properties of newly synthesized polymers [96,97], namely isotactic and syndiotactic poly(*N*-pentenyl-carbazole) (i-PPK and s-PPK), and the electroluminescence spectra of devices fabricated by using them as EMLs. We have demonstrated that the polymer tacticity, along with the proper design of the layer structure, strongly affects the OLED's photoconductive properties [98,99]. In particular, we have succeeded in obtaining white light emission with a single EML based on isotactic polymer i-PPK in a multilayer OLED (Figure 6a). The white light emerged from three contributions, as shown in the electroluminescence (EL) spectra in Figure 6b, which were associated with three distinct phenomena: fluorescence from an electroplex (an intermolecular complex formed under an electric field) across the EML and HBL interface, phosphorescence from the excimer (an arrangement of two carbazole-overlapping groups), and emission due to the electromer (an excimer formed in the presence of an electric field) (Figure 6c). Conversely, OLEDs based on i-PPK with a monolayer structure and

based on the syndiotactic polymer emitted blue light, which originated from excimers (Figure 6d) [100,101].

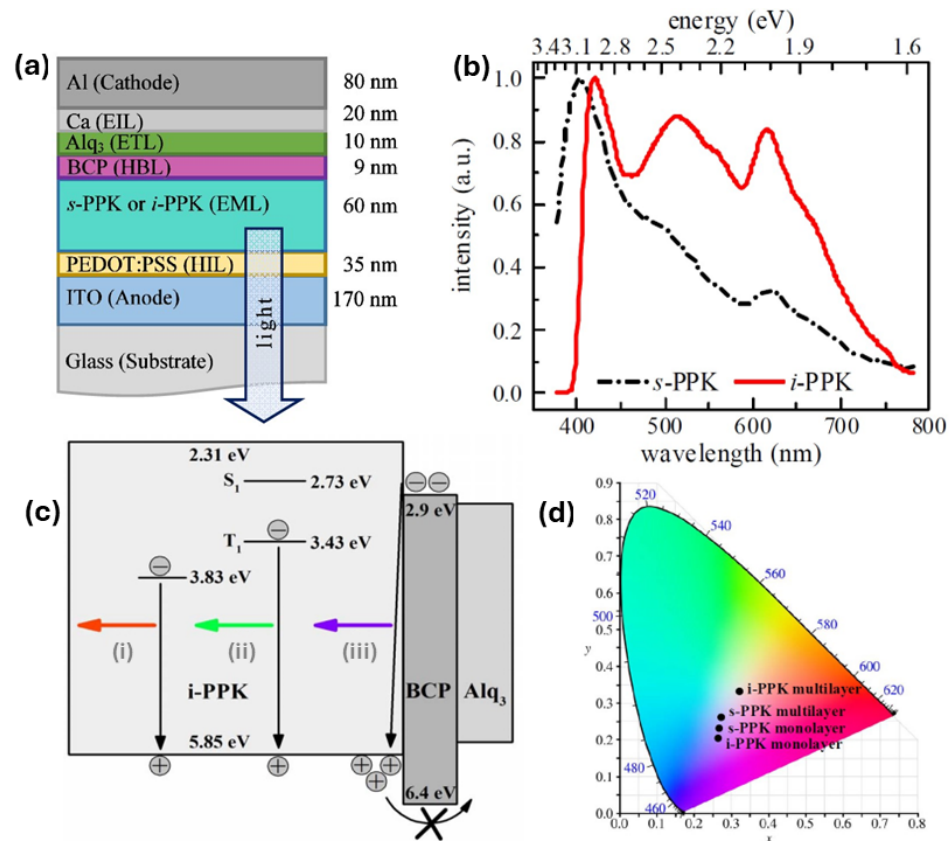


Figure 6. (a) Scheme of fabricated multilayer OLEDs based on s-PPK and i-PPK, emitting blue or white light; the structure without HBL and ETL is referred to as a monolayer structure. (b) Normalized EL spectra of multilayer OLEDs at 5 mA. (c) Energy diagram of i-PPK-based OLED with emission mechanisms due to (i) electromers, (ii) triplet excitons, and (iii) electroplexes; excited states refer to the partially overlapping excimers. (d) CIE coordinates of mono- and multilayer PPK-based OLEDs.

The quality of the light generated by a WOLED depends on the ability to reproduce the object color. This characteristic not only has aesthetic benefits but also plays a crucial role in many applications, ranging from monitoring a system or process for predictive maintenance to lighting's impacts on health. In this regard, several studies have shown that OLEDs, containing no UV light and having low content of blue light, have benefits for the circadian rhythm and cognitive abilities. OLED devices were created with tunable chromaticity by appropriately controlling the relative emission intensity of four complementary emitters. In particular, it was possible to easily obtain CCT ranging from 5200 K to 1580 K, by modifying the thickness of the emissive layers and with the use of an additional carrier-modulating layer (CML) and by adjusting the applied voltage. In this way, the device CCT covered that of cool and warm light for daylight illumination, and even reached that of dusk hue (2500 K) and candlelight (1900 K) in order to provide physiologically friendly illumination at night with the lower emission of melatonin-suppressing components [102]. To this end, a recent project has been dealing with the development of WOLEDs whose CCT can be tuned between 2700 and 5000 K over one decade of current from 50 to 500 mA. The aim was to bring, among various applications, benefits to the healthcare sector, where cooler illumination can help nurses and doctors to stay alert during the daytime, while warmer light promotes rest during night [103]. Similarly to the achievements made in display applications, an effective technique to achieve tunable white light can be dynamic driving, such as pulse width modulation (PWM), controlling the duration for which the OLED is turned on, or an AC voltage with a variable amplitude [104]. Figure 7 shows the EL spectra,

the corresponding CIE coordinates, and photos of a WOLED with an n-i-p-i-n structure, driven by a square wave voltage at a frequency of 50 Hz and a duty cycle of 50%. Here, by changing the polarity of the voltage, one of the p-i-n junctions is activated; therefore, by modulating the positive and negative amplitudes, it is possible to achieve a combination of blue and red light, thus tuning the color of the resulting white light.

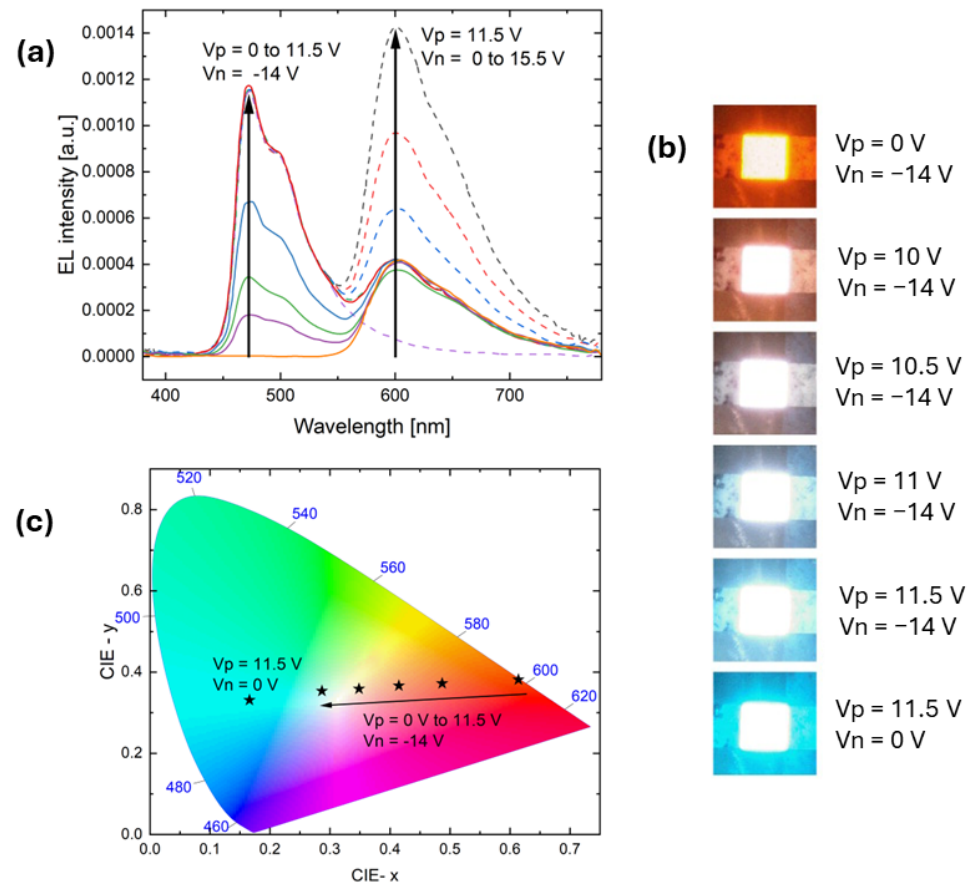


Figure 7. (a) EL spectra of an OLED driven with variable positive or negative amplitude AC voltage. (b) Photographs of the device under different voltage amplitudes. (c) Variation in CIE coordinates of devices shown in (b). Reproduced with permission from [104]. Copyright 2000, Elsevier Science & Technology Journals.

Finally, it is important to ensure that the light characteristics remain stable both under varying brightness and over time. Indeed, the majority of WOLEDs undergo a color shift due to the variation in the emission peak ratio of various chromophores, both due to the applied voltage and the degradation over time of some components. For this reason, recent research has focused on studying WOLEDs based on a single organic molecule or aggregates, demonstrating high efficiency, color stability, and ease of fabrication. The white light originates from the combination of high-energy emissions, resulting usually from excited states of $\pi-\pi^*$ transition, and of low-energy emission generated from dimers or excimers, incomplete energy transfer, intramolecular charge transfer such as exciplex, and metal-to-metal interactions [105–109]. The issues discussed so far related to WOLED performance for lighting applications and the proposed solutions in the literature are summarized in the diagram shown in Figure 8.

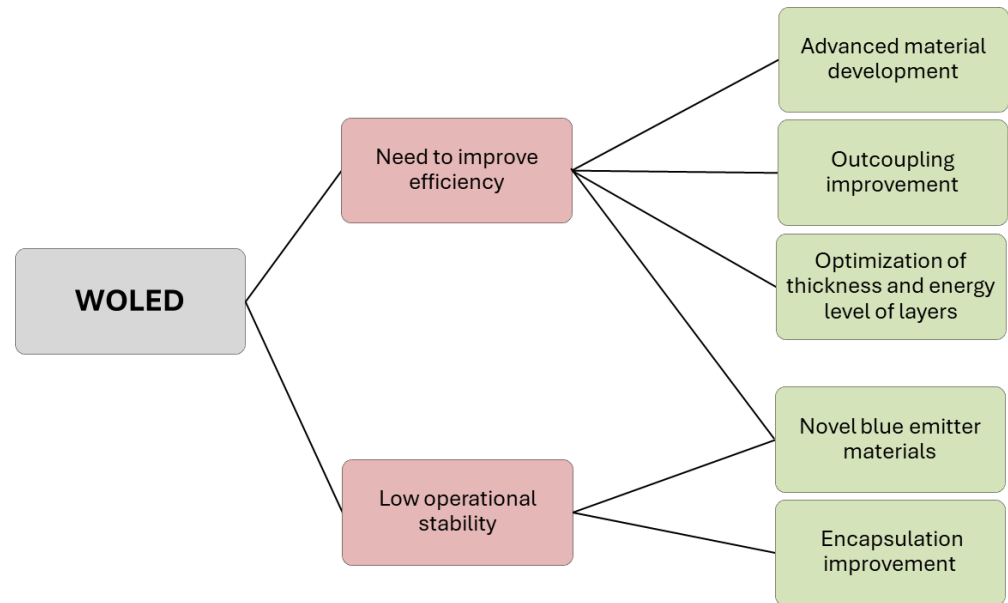


Figure 8. Main issues related to the realization of white OLEDs (red boxes) and possible solutions (green boxes) to be adopted.

4. Challenges in OLED Transparency

Transparent OLEDs (TrOLED) allow bidirectional light emission. The multilayer structure of a TrOLED is created on a transparent substrate of glass or other plastic materials, a transparent anode, different functional layers, and a transparent cathode. Like conventional opaque OLEDs having only one transparent electrode serving as a window of light, transparent OLEDs can be classified based on the emitting structure in standard and inverted devices. In particular, a standard TrOLED is defined as having a top-cathode/bottom-anode configuration, whereas, in an inverted TrOLED, the anode and cathode are the top and the bottom electrodes, respectively (Figure 9) [25].

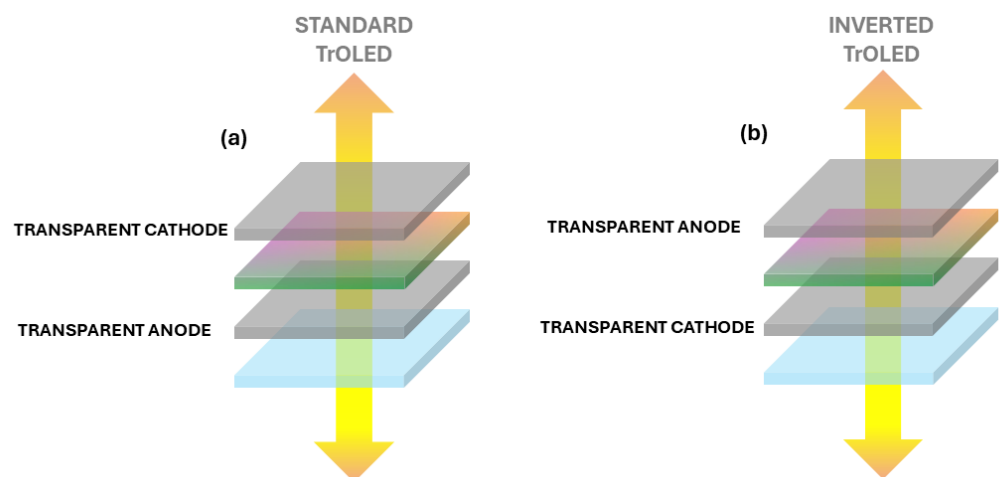


Figure 9. Structures of a transparent (a) standard OLED and (b) inverted OLED.

The prerequisites necessary to have a transparent electrode that also provides good electrical contact are high transmittance in the visible range and high conductivity. However, achieving both of these simultaneously poses a challenge, leading to an inevitable trade-off.

The optical transmittance T of a thin film is related to its thickness t and its absorption coefficient α through the Beer–Lambert Law:

$$T = e^{-\alpha t}. \quad (1)$$

As the thickness of a film rises, the optical transmittance falls. The conductive properties of the contact are instead indicated by the sheet resistance, R_s , defined as

$$R_s = \frac{\rho}{t}, \quad (2)$$

where ρ is the resistivity. Therefore, to reduce R_s and thus the voltage drop along the contact surface, it is desirable to use materials with low resistivity and a greater layer thickness. Additionally, the transparency and conductivity of an electrode can be influenced by surface and interface effects such as roughness, patterning, and optical interference, as well as the conditions under which the materials are synthesized and processed [110].

Over the years, numerous alternative transparent conductive materials have been studied and utilized as electrodes for organic optoelectronic devices, specifically in organic photovoltaic (OPV) and OLED devices. It is possible to classify them into four macro-groups (Figure 10): transparent conductive oxides (TCO), thin metal layers, transparent conductive polymers, and nanoscale materials. Among the alternatives, the two classes of materials most widely used to produce electrodes are TCOs and thin metal layers, which will be analyzed in more detail below.

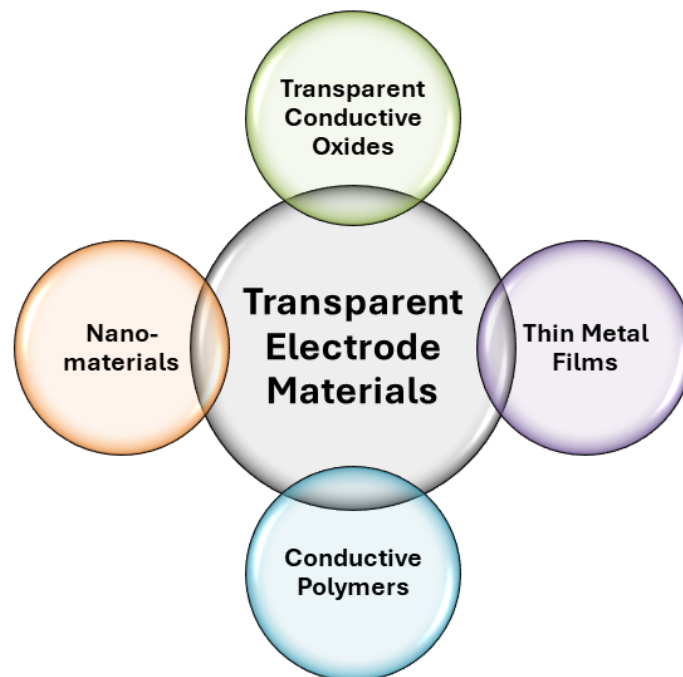


Figure 10. Different categories of materials employed in the fabrication of transparent electrodes for optoelectronic devices.

Conducting polymers such as polyaniline, polypyrrole, and polythiophene with the appropriate chemical dopants are organic materials with great transparency, electrical conductivity, and flexibility. They offer several advantages over other electrode materials, including their lightweight nature, mechanical flexibility, easy solution processability, and exceptional compatibility with plastic substrates. Among them, PEDOT:PSS is a very successful and extensively utilized conducting material for optoelectronic transparent electrodes [111]. Nevertheless, conductive polymers still exhibit poor stability when exposed to high temperatures, humidity, and UV and offer an imbalanced combination of sheet

resistance and transparency when considered individually (without being combined into a composite) [112]. However, when used in composite materials, they demonstrate improved performance [113]. Further improvements are necessary to surpass the performance of other transparent conductive electrode materials, mainly when used in large-sized, commercial-scale devices [110].

Over the past two decades, extensive research has been conducted also on nanoscale materials, focusing on their controllable synthesis and attractive applications in various fields. Several of them, including graphene, carbon nanotubes (CNTs), and metal nanowires (NWs), possess appealing optoelectronic characteristics, making them highly promising for use as transparent conductive electrodes (TCEs). Some of the nanomaterials are also compatible with solution-based and large-scale manufacturing processes [114].

Graphene has attracted significant attention due to its distinctive characteristics, such as great optical transparency, low sheet resistance, and exceptional mechanical flexibility, and can be utilized as a flexible electrode in wearable systems [115]. Researchers have intensively investigated various techniques to produce high-quality graphene at a low cost. One promising advancement in the practical application of graphene as an electrode is the development of a roll-to-roll process for the large-scale production and transfer of the film, but the use of graphene still faces some challenges that require development. These include poor adhesion to substrates and low electrical conductivity compared to other TCE materials [116]. Carbon nanotubes, which are cylindrically structured nanoscale-diameter materials, represent another promising option for use as TCEs because of their excellent electrical and mechanical properties, flexibility, and appropriate work functions. Nevertheless, they exhibit significant sheet resistance and substantial roughness that affects the carrier mobility and reduces the lifetime of the device [117]. Thus, there is still a need for an appropriate method to develop a high-conducting and transparent CNT film for large-scale production. Transparent electrodes consisting of randomly dispersed networks of metal NWs, such as silver (Ag) or copper (Cu) nanowires, have also been documented to exhibit elevated optical transparency, low sheet resistance, and exceptional mechanical flexibility. These materials can be produced using a cost-effective roll-to-roll manufacturing method, while maintaining the high conductivity of the metal [118]. However, this type of nanomaterial is susceptible to moisture and external mechanical damage, and their ability to adhere to the plastic substrate is still inadequate [119,120].

Below, the other two types of TCEs are examined in detail, both of which are well suited for the maintenance of the metal's high conductivity and for use in TrOLEDs for lighting applications. The discussion starts with the deposition method, analyzing the advantages and challenges of each type, and provides a performance comparison in terms of transparency and sheet resistance. Additionally, it addresses compatibility with flexible and large-area substrates.

4.1. Transparent Conductive Oxides

The most common transparent conductive contacts, extensively studied for OLEDs and other organic optoelectronic devices, are TCOs. They are highly doped metal oxides (SnO_2 , In_2O_3 , ZnO , CdO) that offer remarkable transparency, with transmittance not lower than 80% in the visible spectral range, due to the wide bandgap of oxides. At the same time, they allow for conductivity as high as 10^4 S/cm due to the introduction of dopants [41,121].

TCO films are prepared by different coating techniques: physical methods such as radio frequency (RF) sputtering and electron beam evaporation and chemical methods such as spray pyrolysis, sol-gel, or atomic layer deposition (ALD). Compared with other coating methods, sputtering presents evident advantages: reproducibility, a high deposition rate, high film quality, and good large-area uniformity. Moreover, sufficient throughput should be ensured to employ alternative techniques, such as ALD, in mass production.

The majority of reported TrOLEDs employ indium tin oxide (ITO) electrodes as a bottom contact, thanks to the film's excellent quality, transparency, work function, and electrical conductivity. ITO is a doped metal oxide composed of 90% In_2O_3 and 10% SnO_2 that

is usually deposited by a sputtering process that, along with a high substrate temperature, allows the maximization of both the electrical conductivity and optical transparency at the same time [122,123]. Other techniques adopted in most of the commercialized ITO films are chemical vapor deposition and solution procedures [124,125]. The characteristics of this material make it attractive for the realization of the top contact, but this is hindered by the damage caused to the underlying sensitive layers of the device during its deposition via sputtering, due to plasma emission and particle impacts. Therefore, the use of ITO for both electrodes in TrOLEDs is still challenging.

The primary reason for the sputter damage during TCO deposition is the bombardment of the substrate by very energetic particles; the key species involved in the process are ions sputtered from the target surface, negative ions generated within the plasma, electrons generated on the target surface, positive ions produced in the plasma, reflected atoms, and neutralized ions from the target surface. Among these damage factors, ions and secondary electrons have the highest energy, which has been demonstrated to cause much greater damage to the organic layers. The development of a sputtering process with less damage and that operates at low temperatures is crucial in improving the performance and lifetime of such devices [126]. The optoelectronic properties of ITO strongly depend on the process parameters, such as the substrate temperature, sputtering power, process pressure, deposition time, and any post-process annealing treatments.

A possible widely studied solution to better control or avoid damage is the introduction of a pre-deposited thin buffer layer between the ITO and organic layers, with the additional advantage of enabling efficient carrier charge injection from the ITO into the adjacent organic layer. Metal-based protection layers such as Mg-Ag or Ca thin films have been demonstrated as good protective layers that enhance the electron injection, but they can result in a reduction in the total transmittance of the device [127,128]. Transition metal oxides (TMOs), like MoO₃, WO₃, V₂O₅, Rubrene, and NiO, are used for efficient hole injection in the buffer layer; however, some of them need relatively high deposition temperatures or require deposition processes that are harmful to the underlying organic layers [129,130]. Organic buffer layers, e.g., copper phthalocyanine (CuPc), Bphen, or pentacene, can offer good transmittance, but their polycrystalline structures result in a reduction in their conductivity [131,132].

An example of a transparent OLED with both ITO electrodes, which employs a TMO buffer layer, is reported in [130], where an inverted architecture is adopted. To safeguard the organic materials from particle-related issues during the deposition of the ITO anode as the top electrode, a buffer layer of WO₃ is incorporated. The device exhibits average transmittance of 75% in the visible range, with a peak of 90% at about 450 nm. The optimal thickness identified for WO₃ is 60 nm: thicknesses below 20 nm fail to shield the underlying organic layers adequately during ITO sputtering, while thicknesses exceeding 80 nm do not improve the protection against sputtering damage.

In light of the scarcity of indium resources, extensive efforts have been undertaken to create transparent conductive oxides that do not rely on indium. An alternative TCO, although not as widely used as ITO due to its lower conductivity and transmittance, is fluorine tin oxide (FTO). This material has some advantages over ITO: it is more stable, no diffusion into organic materials is reported, and its properties are independent of the cleaning methods used [129]. Zinc oxide (ZnO) is another desirable substitute for ITO since it has a large amount of material storage, and it is transparent in the visible spectral range and non-toxic to the environment. In order to improve the film's conductivity, extrinsic dopants such as Al (AZO—Al-doped ZnO) or Ga (GZO—Ga-doped ZnO) are introduced, giving material properties such as transparency and conductivity that are comparable with those of ITO [133]. Silva et al. [134] reported an optimized AZO thin film to be used in organic electronics with electrical resistivity of $4.9 \times 10^{-4} \Omega \cdot \text{cm}$ and average transmittance of 92% in the visible region (400–700 nm). An AZO-based test OLED showed electro-optical performance comparable to the ITO-based reference device in terms of the luminance and turn-on voltages.

The representative transmittance and sheet resistance values of different types of transparent electrodes reported in the literature, including TCOs, are shown in Figure 11.

In summary, despite being the dominant electrode for optoelectronic devices, TCOs, and particularly ITO, face several challenges, especially for large-area applications, where the escalating cost of the material, driven by indium's scarcity and high consumption, for mass production continues to be a barrier. The elevated temperatures required by the fabrication processes and the damage caused by high-energy deposition to the underlying organic materials limit ITO's application in flexible and lightweight OLED devices. In addition, ITO's high rigidity and brittleness would not guarantee durability against mechanical deformation. The frequently used magnetron sputtering method for the realization of top transparent electrodes causes inevitable damage to soft organic films. Implementing a protective layer remains the most favored approach to minimizing or alleviating the consequences of sputter damage. The optimization of the sputtering process, which is the most well-established method of producing transparent electrodes, remains mostly unexplored.

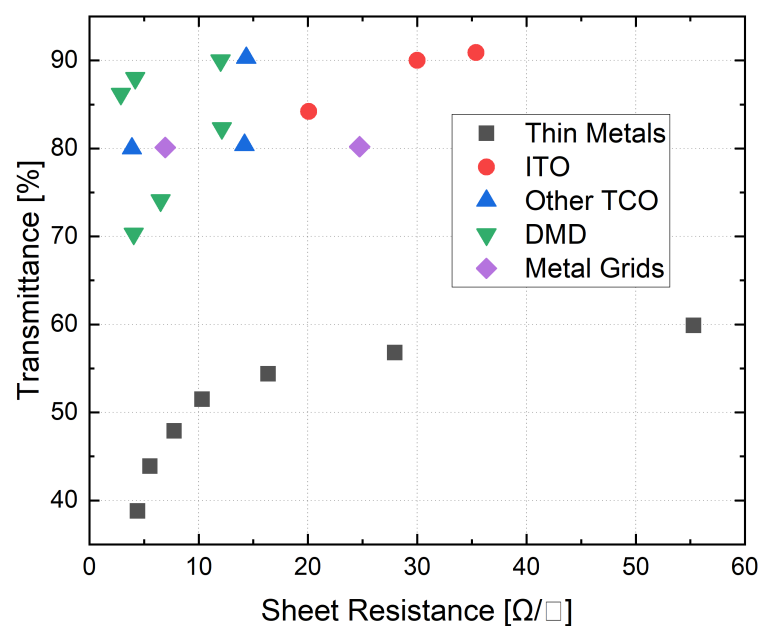


Figure 11. Transmittance values in the visible spectral range as a function of the sheet resistance reported in the literature for ITO [111,135,136], other TCOs [133,137,138], thin metal layers [139–142], DMD multilayers [143–146], and metal grids [147,148].

4.2. Thin Metal Films

A metal layer, such as gold, silver, or aluminum, can be made semi-transparent to visible light and thus serve as a substitute for TCO for the realization of an OLED top transparent contact, if its thickness is reduced below 20 nm. This is referred to as an ultrathin metal film (UTMF). Certainly, metals facilitate ohmic charge injection into organic charge transport materials; however, their maximum transparency is strongly limited. Considerable effort has been made to preserve the excellent conductivity of ultrathin metal films by ensuring continuity in the film's morphology while enhancing their transparency.

UTMF can be deposited using a variety of physical vapor deposition (PVD) techniques, such as thermal evaporation in a high vacuum, which is a low-substrate-temperature process and negligibly affects the underlying layers [149]. Another promising but far less developed method of obtaining a metal film with excellent conformality and good large-area uniformity is atomic layer deposition (ALD) [150]. Finally, roll-to-roll manufacturing enables the deposition of metals onto large-area flexible plastic substrates [151].

Among the noble metals, silver (Ag) and gold (Au) are excellent case studies, which, at a thickness of 10 nm, show average visible transmittance of 43% and 50%, respectively, while ensuring sheet resistance of 20.3 Ω/□ and 40 Ω/□, respectively [152,153]. Other

metals that are widely used for the realization of a transparent electrode are aluminum (Al) or alloys like Mg:Ag, ytterbium (Yb):Ag, and Ca:Ag, which, in the best case, guarantee transmittance comparable with that of ITO and sheet resistance of about $50 \Omega/\square$ [154]. Alkaline and alkaline-earth metals such as calcium (Ca) and cesium (Cs), due to their low work functions (2.9 eV and 2.1 eV, respectively), which facilitate the injection of electrons into organic materials, are excellent candidates for a cathode electrode. However, these metals with low work functions are highly reactive with air and even with small organic molecules, a factor that prevents them from maintaining their metallic state in the long term [37]. Consequently, few research activities have reported employing alkaline-earth metals as the transparent conductive layers in optoelectronics, despite their advantageous transparency and conductivity as well as excellent electron injection capabilities.

Among the listed cases, Ag is the one that exhibits the highest transmittance. A critical aspect to overcome to make it a suitable option for a transparent metal electrode is achieving perfect surface coverage at low thicknesses, i.e., a 2D continuous silver film capable of ensuring good conductivity and promoting charge injection. The silver layer normally follows the 3D island formation method known as Volmer–Weber growth [155], in which Ag agglomeration occurs due to the stronger cohesive forces among Ag clusters compared to the adhesion forces at the metal and substrate interface. This prevents the precise deposition of a single ultrathin Ag film with low resistivity and good uniformity. The imperfect electrical path connection caused by Ag agglomeration typically leads to increased sheet resistance, resulting in lower transmittance at the desired thickness of Ag with suitably low sheet resistance.

Since the surface coverage also depends on the surface energy of the underlying layer, it may be useful to deposit a seed layer before the silver one, able to promote the wetting effect on the deposition surface for the controlled layer-by-layer growth of the metal film [156]. By increasing the adhesion force at the interface, the seed layer can decrease the coalescence between Ag clusters without compromising the optical transparency. Recently, in [157], a highly transparent and low-sheet-resistance electrode was designed by preceding the deposition of an 8 nm silver cathode with a ZnS-based seed layer deposited via thermal evaporation to enhance the surface energy of the substrate. While, in the absence of the seed layer, a minimum thickness of 15 nm would have been required to achieve sheet resistance lower than $10 \Omega/\square$, the silver electrode with an 8 nm thickness produced on a ZnS-based seed exhibited sheet resistance of $6.4 \Omega/\square$. The latter, with the addition of a capping layer (CL)—an outer dielectric layer with a high refractive index, used to reduce the reflection effect of the metal electrode—also based on ZnS, was used to fabricate the cathode of a 1 cm^2 blue transparent OLED, whose anode was formed by ITO. This resulted in overall transmittance of 91%, which is close to that of the only ITO anode film.

In order to modify the adhesion force at the deposition surface, other techniques are also used, such as oxygen plasma, ultraviolet–ozone treatment, and thermal annealing. In [158], a symmetrical bottom and top emission device is implemented with a 6 nm Ag bottom contact obtained by using oxygen plasma treatment before the deposition of a nanoscale thin Ag layer on glass. The treatment leads to an increase in surface energy, producing a thin and uniform Ag film with low sheet resistance of about $15 \Omega/\square$ and high optical transmittance ($T \approx 76\%$).

Another way to reduce the 3D island formation of Ag atoms during thin-film deposition is to dope silver with metal atoms to form an alloy. In [159], transparent top contacts obtained by Ag:Ca are examined as a possible alternative to TCOs. Different combinations of the co-deposition of calcium and silver are analyzed to obtain intermixed alloys where Ca behaves as a transparent surfactant, enhancing the surface wettability and therefore favoring the growth of highly conductive Ag. The best performance is exhibited by the combination of a 1 nm Ag underlayer with a Ca:Ag (MR 1:1) film, showing visible transmittance of 76% (between 380 and 780 nm) and sheet resistance of $27.1 \Omega/\square$. The electro-optical performance of a co-deposited layer is nearly identical to that of TCO, with the benefit of being processed by evaporation onto organic materials. A more recent experiment has

achieved higher optical transmittance, reaching 88.4% for the electrode, by depositing an ultrathin and smooth Cu-doped Ag film of 6.5 nm on a flexible polyethylene terephthalate (PET) substrate [160]. In [161], a reliable transparent cathode was investigated, obtained by the co-deposition of silver and aluminum on a LiF/Al seed layer using thermal evaporation. During the deposition process, the thin Al layer functioned as a seed layer to minimize the Ag island growth mode and, furthermore, dissociated LiF (lithium atoms acted as dopants for the ETL layer), enhancing the electron injection property of the electrode. The contact obtained in this way showed sheet resistance lower than $7.0 \Omega/\square$, while the Al doping of Ag ensured high-temperature reliability and stability. A green phosphorescence TrOLED with an active area of $2 \times 2 \text{ cm}^2$ was fabricated by employing a transparent Ag:Al cathode, a p-bPPhenB capping layer, and an ITO anode. The maximum transmittance of the device was 81.2% at 520 nm, while the average transmittance in the visible range was 72.0%; see Figure 12.

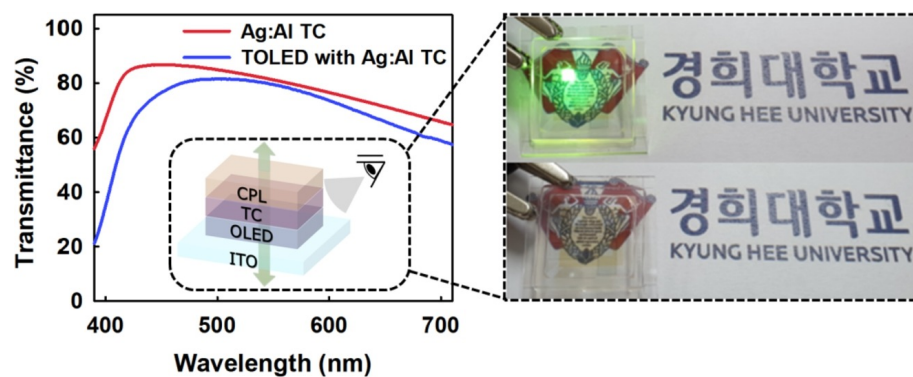


Figure 12. Transmittance of transparent Ag:Al electrode and of the whole device on the left; photograph of the ON (4 V) and OFF TrOLED on the right. Reproduced with permission from [161]. Copyright 2000, Elsevier Science & Technology Journals.

Ultimately, one way to improve the transparency of metallic films while maintaining optimal conductivity is to use them not alone but in combination with other layers. An extensively studied multilayer structure is the dielectric/metal/dielectric (DMD) configuration, considered a valid alternative to TCO in obtaining transparent electrodes in next-generation OLEDs. It consists of a thin metallic film sandwiched between two antireflection dielectric layers to achieve high transparency. The two dielectric layers increase the overall transparency thanks to surface plasmonic effects at the two metal/dielectric interfaces and optical interference within the multilayer structure, while the intermediate thin metal layer ensures the electrical conductance of the entire structure. The optical properties of a multilayered film may be controlled by matching the refractive indices of its different layers. Light creates an electromagnetic field at each layer boundary as it travels through a stacked thin film, as in OLEDs. In other words, the transmittance of multilayered thin films, defined as the ratio between the incident and transmitted electromagnetic field, is determined by considering the boundary conditions and phases of the electromagnetic field in each layer [162].

The DMD structures employed as electrodes for TrOLEDs do not necessarily require plasma procedures during manufacturing, eliminating the need for a thin protective film for the underlying organic layers. Conversely, it is possible to employ the thermal evaporation process, which, in addition, allows the thickness of the dielectric layer to be controlled to provide good transmittance within the chosen wavelength spectrum [163]. As a result, various studies have successfully achieved both low sheet resistance and high transmittance; however, when implemented in practical TrOLEDs, DMD electrodes continue to face stability and efficiency issues. Indeed, the optimization of the DMD structure should not only consider the transmittance but also the overall cavity structure and its correlation with the emission spectrum of the emitter molecules, given that each layer of the structure has

distinct optical characteristics. The adjustment of the dielectric capping layer thickness contributed to both high transmittance and the improved stability of the silver electrode.

The metals frequently used in multilayer structures are Ag and Au, while the most common oxide layers are (WO_3) and ZnO, but also ITO or FTO are used. Various configurations have been reported in the literature; the most commonly used are MoO_3/Ag or Au/MoO_3 [164–167], $\text{MoO}_3/\text{Ag}/\text{WO}_3$ [143], $\text{ZnS}/\text{Ag}/\text{WO}_3$ [168], $\text{ZnS}/\text{Ag}/\text{MoO}_3$ [169], $\text{ZnS}/\text{Ag}/\text{ZnS}$ [170], ZnO/Ag or Au/ZnO [171–175], $\text{FTO}/\text{Ag}/\text{FTO}$ [176], ITO/chAg or Au/ITO [175,177], and $\text{AZO}/\text{chAg}/\text{AZO}$ [178].

The structure $\text{ZnO}/\text{Ag}/\text{ZnO}$ has been considered among the most promising options for a transparent cathode, thanks to the attractive properties of ZnO, such as high transparency in the visible range, relatively high electron mobility, environmental stability, and a high refractive index, serving as a capping layer and simultaneously as an encapsulation layer [175]. Moreover, recently, it has been studied to enhance its performance [179]. Here, a highly transparent cathode with the structure of $\text{ZnO}/\text{Mg:Ag}/\text{ZnO}$ was employed to fabricate a green TrOLED. In particular, ZnO had the role of protecting the ultrathin Mg:Ag alloy layer while preserving the low work function of the electrode. The cathode transparency of 84.6% in the visible light range allowed an increase in transmittance by 20% compared to that shown by the reference devices obtained with Mg:Ag cathodes. The electrode was deposited by a low-temperature ALD and laminating procedure, techniques that are gentle enough to avoid any damage to the underlying organic layers [180].

Metal oxides, especially (MoO_3) or WO_3), when deposited by thermal evaporation, generally require high-temperature processes and therefore are not compatible with plastic substrates, for which organic dielectrics are more suitable due to their lower deposition temperatures.

In [181], a comparison was reported between the most common DMD structure, $\text{MoO}_3/\text{Ag}/\text{MoO}_3$, and an organic/Ag/organic electrode for application on a flexible poly(ethylene terephthalate) (PET) substrate. The organic-material-based structure was made of a thin 12 nm Ag layer grown on an organic wetting inducer layer of 1,4-bis(2-phenyl-1,10-phenanthroline-4-yl)benzene (p-bPPhenB) and covered with an organic antireflective capping layer of 1,4,5,8,9,11-hexaazatriphenylene hexacarbonitrile (HATCN); it showed 81.34% transmittance at 550 nm and significantly low sheet resistance of about $9.51 \Omega/\square$, while the MoO_3 -based electrode had relatively lower transparency with peak transmittance of about 67.18% and higher sheet resistance of $13.51 \Omega/\square$. The organic/Ag/organic electrode also revealed greater mechanical flexibility and durability than the MoO_3 -based electrode on the PET substrate under continuous bending stress.

Another example is an electrode made with a 16 nm Ag film sandwiched between two 30 nm p-bPPhenB layers, acting as both a wetting layer and capping layer, which has proven to be a thermally stable and electro-optically efficient transparent cathode for a top emitting OLED, ensuring very low sheet resistance ($2.1 \Omega/\square$), high transmittance of 83% at 550 nm, and uniform surface coverage [182].

Wrzesniewski et al. reported an interesting study of the dependence of the peak of the transmittance spectra on the type and thickness of the metal used in a DMD structure [166]. They studied a $\text{MoO}_3/\text{metal}/\text{MoO}_3$ trilayer structure. The transmittance peak was shifted to the blue (400–500 nm) region of the visible spectrum when Ag was utilized as the intermediate layer. When the metal layer was replaced with Au, the peak transmittance shifted toward the green and red (550–600 nm) portions of the spectrum. By stacking ultrathin layers of Au and Ag in this structure, it was possible to broaden and tune the transmittance peak by altering the thickness of each layer (Figure 13). By modifying the composition of the metal intermediate layer, the transparency of this electrode structure can be adjusted to suit various specific applications and emissive molecules. The sheet resistance of trilayer structures with Au/Ag composite intermediate layers is within the range of 12 to $16 \Omega/\square$, which is slightly greater than that of a trilayer with a 10-nm-thick Au intermediate layer, which is approximately $9 \Omega/\square$.

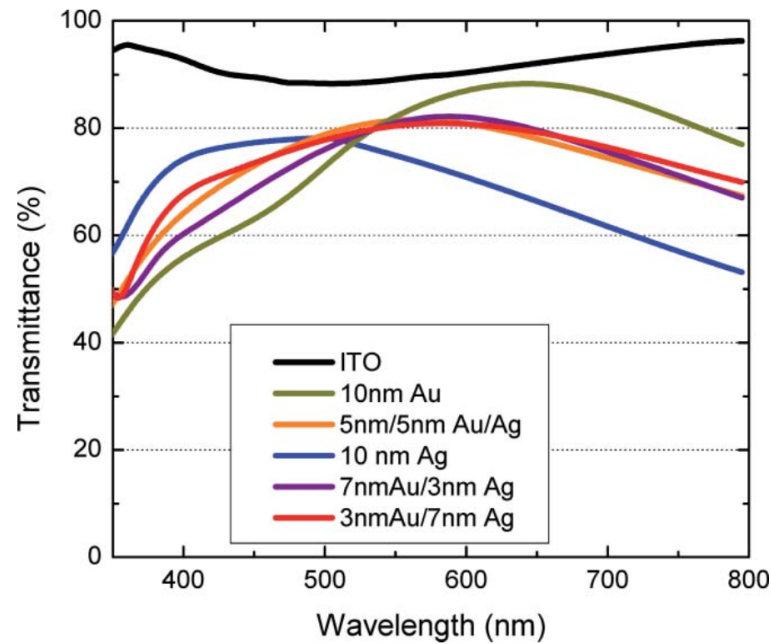


Figure 13. Dependence of transmittance on wavelength for a multilayer structure $\text{MoO}_3/\text{metal}/\text{MoO}_3$ with Ag, Ag/Au, Au metal layers. Reproduced with permission from [166]. Copyright 2011, SPIE.

Another aspect of primary importance when creating transparent OLEDs is the light outcoupling efficiency. Enhancing this figure of merit while preserving their excellent transparency and electrical performance is one of the key challenges that researchers encounter. Improved transmission, decreased (or enhanced) reflection, decreased absorption, and suppressed surface plasmon polaritons all contribute to the outcoupling increase. Different methods have been reported to control the optical properties of an OLED: the insertion of nanostructured scattering layers, low-index grids, or single or double capping layers [183], and the use of high-refractive-index substrates [23,184,185]. Many studies show that the application of an index-matching capping layer (CL), covering the top contact of a device, allows precise control of the TrOLED's bidirectional emission, enhancing the transmittance thanks to plasmon suppression and absorption reduction [186–188]. The efficiency improvement due to the CL insertion could be attributed to the modification of the optical structure that controls the microcavity effect and to the redistribution of the emitted light [189]. With the growing refractive index of the CPL material, the microcavity effect of the device can be adjusted to reduce the light energy loss in TrOLEDs and provide greater control over the device optical characteristics. Although the microcavity effect is a phenomenon that enhances the color purity and optical efficiency, it causes a color shift at large viewing angles; therefore, a trade-off between optical efficiency, color purity, and angular color shift is necessary in the design of an OLED [190]. The amount of light emitted from the top contact of an OLED is highly dependent on the thickness of the capping layer and the refractive index of the material chosen. The higher-refractive-index capping materials increase the device's top emission properties of luminance and power efficiency [156]. In [111], the light emission properties of a transparent OLED were greatly improved without compromising the device's bottom-side light emission characteristics by using a 40-nm-thick MoO_3 CL. The transmittance in the visible range of the device thus produced was doubled compared to that of the uncapped device.

Table 2 displays the most common materials utilized to create a capping layer, along with their corresponding refractive indices at 550 nm, as reported in literature.

Table 2. Most commonly used capping layer materials with respective refractive indices evaluated at 550 nm, as reported in the literature.

Material	Refractive Index at 550 nm	Ref.
ITO	1.9	[191]
ZnO	2.0	[192]
ZnS	2.3	[193]
ZnSe	2.5	[189]
TiO ₂	2.3	[189]
MoO ₃	2.16	[181]
WO ₃	2.1	[194]
Al ₂ O ₃	1.6	[192]
Alq ₃	1.75	[195]
p-bPPhenB	2.2	[181]
NPB	1.8	[195]
TPD	1.9	[156]
HATCN	1.82	[195]

4.3. Performance of a Transparent Electrode

High optical transmittance and low sheet resistance are the two primary functional characteristics and prerequisites for a TCE, and maintaining a balance between these two attributes is a crucial task. A unique efficient figure of merit (FOM) for TCEs was defined to quantify the performance of a transparent contact in terms of transparency and conductivity by Haacke in 1976 [196], namely $\phi_H = T^{10} \setminus R_s$, where T indicates the transmittance at 550 nm, corresponding to the maximum of photopic vision, and R_s is the sheet resistance. High values of ϕ_H indicate high transmittance and low sheet resistance. The exponent of 10 for the transmittance, as introduced by Haacke, in comparison to other previously defined figures of merit [197], allows one to obtain the optimal value for ϕ_H at a given level of conductivity when the transmittance exceeds 90%. In Table 3, the values of resistance and transmittance at 550 nm from the literature are reported for various multilayer DMD structures; for each of them, Haacke's FOM is also calculated.

Table 3. Sheet resistance and transmittance at 550 nm reported in the literature and calculated Haacke's FOM values for different DMD multilayer structures.

Electrode Structure	Layer Thickness [nm]	Substrate Type	Transmittance [T, %]	Sheet Resistance [R_s , Ω/\square]	Haacke's FOM at 550 nm ¹ [ϕ_H , Ω^{-1}]	Ref.
MoO ₃ /Ag/MoO ₃	40/12/40	PET	67.2	13.1	1.43×10^{-3}	[181]
MoO ₃ /Ag/MoO ₃	30/11/30	Glass	87.2	4.54	5.60×10^{-2}	[198]
MoO ₃ /Ag/WO ₃	5/12/40	-	88	4.2	6.63×10^{-2}	[143]
MoO ₃ /Al/WO ₃	30/15/5	Glass	70	7	4.03×10^{-3}	[199]
MoO ₃ /Au/MoO ₃	5/10/40	Glass	82.4	10	1.44×10^{-2}	[166]
ZnS/Ag/MoO ₃	25/7/5	Glass	83	9.6	1.61×10^{-2}	[169]
ZnO/Ag/ZnO	40/18.8/40	Glass	96	4.4	14.9×10^{-2}	[173]
ZnO/Ag/ZnO	-	PET	95.2	10.3	5.93×10^{-2}	[174]
WO ₃ /Ag/WO ₃	40/12/40	-	90	6	5.8×10^{-2}	[200]
ITO/Ag/WO ₃	40/12/40	-	40	6	1.7×10^{-5}	[200]
ITO/Au/ITO	20/8/20	PET	88	16.7	1.67×10^{-2}	[201]
ITO/Ag/ITO	40/12/40	-	27	6	3.4×10^{-7}	[200]
FTO/Ag/FTO	20/7/30	Glass	96.1	-	7.8×10^{-2}	[176]
SiO ₂ /Ag/SiO ₂	40/12/40	-	68	6	3.5×10^{-3}	[200]

¹ Calculated from available data on R_s and T% at 550 nm from graphs.

The table highlights the strong dependence of Haacke's FOM on the transmittance. The latter is minimally affected by the thin metal film, causing only a slight reduction due to the presence of the light pathway, resulting from repeated reflections. Conversely, it

depends on the type of dielectric material and the combination of the dielectric with the metal. In fact, comparing the results obtained from [200] using the same metal but different dielectrics, while the sheet resistance, which depends on the thin metal film, remains the same, the transmittance and therefore Haacke's FOM change significantly with the oxide type. The minimum values, 27% and $3.4 \times 10^{-7} \Omega^{-1}$, respectively, are achieved with ITO, while the maximum values, 90% and 5.8×10^{-2} , respectively, are obtained with WO_3 .

Regarding the dependence on the sheet resistance, it is observed that the structures $\text{WO}_3/\text{Ag}/\text{WO}_3$, $\text{ITO}/\text{Ag}/\text{WO}_3$, $\text{ITO}/\text{Ag}/\text{ITO}$, and $\text{SiO}_2/\text{Ag}/\text{SiO}_2$, having the same thicknesses and deposited by e-beam evaporation, exhibit the same value of R_s , dependent on the metal, regardless of whether the carrier mobility in ITO is greater than that of WO_3 and SiO_2 . For structures with slight differences in thickness, the different R_s values and, consequently, Haacke's FOM values are attributed to variations in the deposition procedures adopted.

The discussed issues for the two types of electrodes and their respective analyzed solutions are schematically outlined in Figure 14.

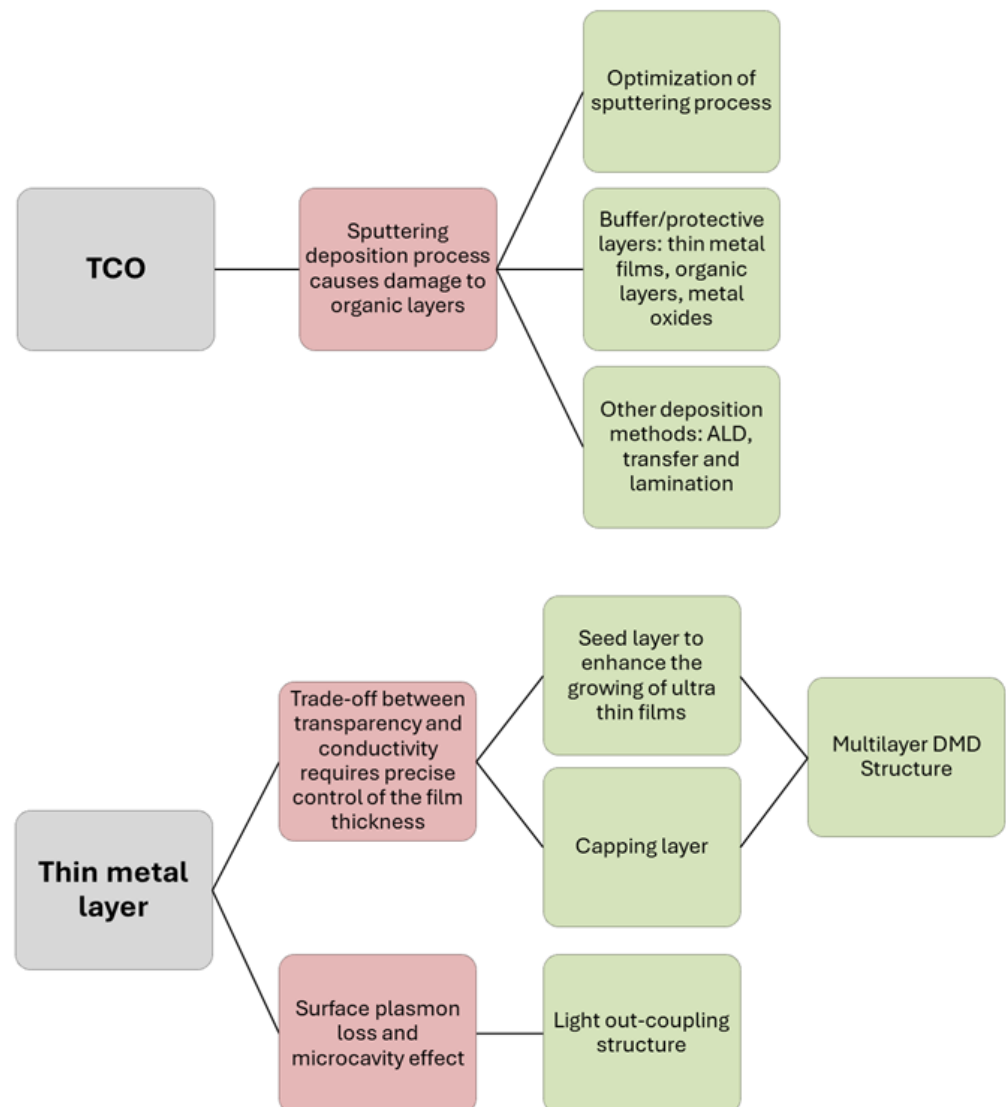


Figure 14. Main issues (red boxes) related to the realization of transparent OLED top electrodes with TCOs and with thin metal films and possible solutions (green boxes).

5. Challenges in Large Areas

A fundamental goal in the latest generation of lighting applications is that of pixel size scaling, aiming to obtain large-area devices while ensuring high performance; in this regard, various issues must be addressed [202]. This specific requirement is one of the factors that has contributed to the slower adoption of OLEDs in lighting applications compared to displays.

First of all, large areas require high driving currents, which are, however, limited by high sheet resistance, as previously highlighted, especially in the presence of transparent conductive electrodes. Additionally, achieving a large area necessitates the use of different methods from those employed in research for small devices, such as spin coating, which must be replaced by more suitable techniques like roll-to-roll printing, transfer, and lamination. Another phenomenon that tends to emerge rapidly with the scaling of the pixel dimensions is device failure due to point defects that arise both when the film thicknesses are very thin and when the surfaces of the underlying layers have high roughness. Consequently, for large-area production, on the one hand, there is the need to increase the film thickness; however, this can result in a degradation in the electro-optical performance. On the other, there is the requirement to adopt specific and high-quality materials, which inevitably leads to increased costs.

As previously illustrated, the color of the emitted light is strictly dependent on the supply current, making it crucial to ensure good conductivity across the entire contact area. Consider, for instance, ITO, which is the most commonly used material for the creation of transparent contacts, mainly the anode. It has excellent transmittance (about 90% at 550 nm) but its sheet resistance value becomes too high for a large-area device, resulting in a significant voltage drop across the anode. As a consequence, it generates a non-uniform distribution of luminance even over lengths of only a few centimeters, which represents a significant aspect in large-area WOLEDs for lighting applications. One of the solutions adopted to reduce the resistance of an anode electrode based on ITO, without compromising the transparency, and thus improving the spatial luminance uniformity across the entire area, is the addition of a metal grid [203–205].

An OLED optimized with a grid can be modeled by including three conductive layers: the bottom electrode with the grid layer, forming the anode, and the top electrode. Since their thickness is negligible compared to the lateral dimensions, their potential is independent of the thickness [206,207]. It is also possible to consider the potential of the grid equal to that of the lower electrode. Under these conditions, the lateral current densities of the grid and ITO are proportional to the field along the electrode and their respective conductivities. Moreover, the lateral current densities are related through the continuity equation to the vertical current of the OLED J_z , obtaining for the potential V_a of the anode, formed by the combination of the two layers, the following equation:

$$\nabla^2 V_a(x, y) = R_a J_z(x, y), \quad (3)$$

where R_a is the equivalent anode sheet resistance, being spatially inhomogeneous and given by

$$R_a = R_b \quad (4)$$

in the absence of the grid and by

$$R_a = R_b \frac{R_g}{R_b + R_g} \approx R_g \quad (5)$$

in presence of the grid. R_b and R_g are the sheet resistances of the bottom layer and the grid, respectively. Therefore, the overall electrode can be seen as a film with a spatially non-

uniform sheet resistance, which, through the efficiency η (cd/A), influences the luminance L , resulting in the same non-uniform distribution.

$$L(x, y) = \eta \frac{\nabla^2 V_a(x, y)}{R_a} \quad (6)$$

Among the various existing grid geometric shapes (Figure 15a), we have studied the hexagonal one, which is the most commonly used compared to triangular or square. This is because it divides the surface into regions of equal area with the minimum perimeter and ensures the best uniformity by generating the smallest voltage drop compared to other shapes. Various types of hexagonal metal grids were compared. In particular, two metals were exploited: silver, with a thickness of 20 nm, and aluminum, with a thickness of 80 nm. For the lateral dimension l of the hexagons (Figure 15b), four values were chosen (1, 2, 4, and 8 nm), while the line width was set to 150 μm for all grids.

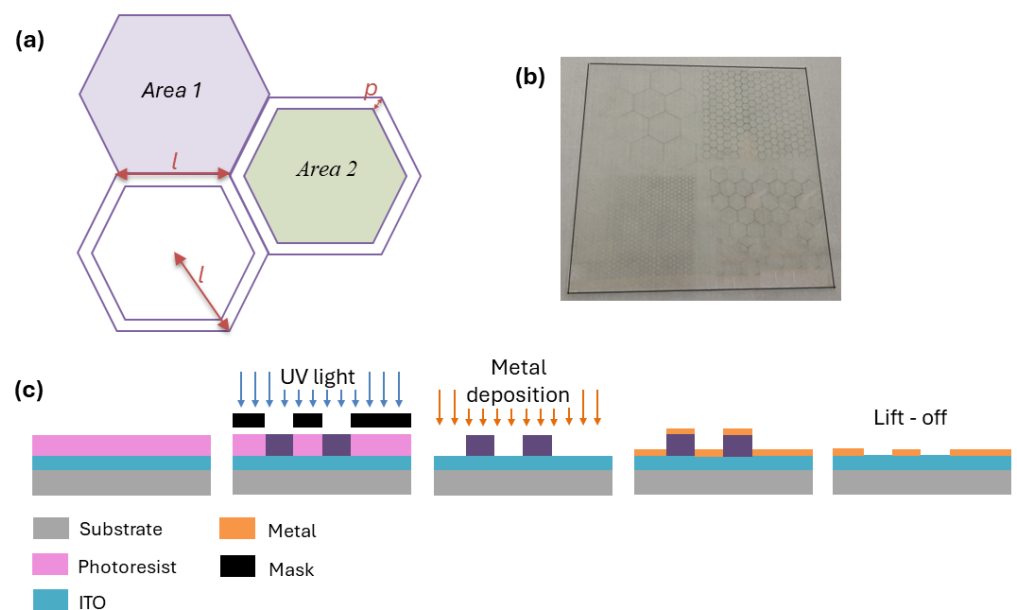


Figure 15. (a) Hexagonal grid structure and dimensions for FF definition. (b) Photograph of the metal grids deposited by the lift-off process, with different dimensions. (c) Lift-off process used for the preparation of the metal grids, consisting of the deposition of a photoresist, the creation of an inverse pattern through UV exposure and etching, metal evaporation, and the removal of the photoresist and metal in excess, obtaining the final metal pattern.

The transparent electrode was commercial ITO, sputtered on glass substrates, after cleaning with deionized water and detergent in an ultrasonic bath and rinsing with acetone and isopropyl alcohol, as well as drying in an oven at 130 $^{\circ}\text{C}$ for at least two hours. All the metal grids were obtained by the lift-off technique (Figure 15c), where a sacrificial photoresist was used to create a new layer with the desired patterns. The sacrificial layer of photoresist was spin-coated onto the substrate. A pattern generator was employed to imprint the metal grid pattern onto the photoresist. Subsequently, a developing solution was used to remove the exposed areas of the photoresist. In the deposition system, the metal was thermally evaporated at a base pressure lower than 5.0×10^{-7} mbar, covering the entire substrate. The sacrificial photoresist, along with the metal on it, was washed away in an acetone bath. This process left only the metal in direct contact with the underlying ITO on the substrate. The electrical sheet resistances of the metal grids on the ITO were measured by a four-point probe and were compared with the optical transmittance measurements, which were obtained using an UV/visible spectrometer in the wavelength range of 400 nm to 800 nm. The width and thickness of the metal lines were measured using an optical profilometer.

The results are summarized in Tables 4 and 5 and reported as a function of the fill factor (FF) in Figure 16. FF is defined as the portion of the area covered by the metal compared to the ITO total area, calculated as shown in Figure 15a, through the following formula:

$$FF = \frac{Area_1 - Area_2}{Area_1} = \frac{l^2 - (l - p)^2}{l^2} \quad (7)$$

where l is the hexagonal side length and p is the distance between two vertices of the inner and outer hexagons. The predicted sheet resistance R_a and the transmittance T_a of the combined electrode can be evaluated as follows [208]:

$$R_a = \zeta \frac{\rho_g}{\tau_g FF} \quad (8)$$

$$T_a = T_{ITO}(1 - FF) \quad (9)$$

where ζ is a correction factor depending on the deposition conditions and it is determined experimentally for a given process; ρ_G and τ_G are, respectively, the resistivity and thickness of the metal. The experimental measurements of T_a are in good agreement with the predictions of Equation (5). In both studied cases, the metal grid is sufficiently thick to be opaque, so that the transmittance of the anodes does not depend on the type or thickness of the metal used, but only on the FF ; therefore, it has the same values for both analyzed grids. As regards the sheet resistance, for the correct estimation of its value, the contribution of the bare ITO, which is of the same order of magnitude as the R_a data (about $12 \pm 2 \Omega/\square$), cannot be neglected. Meanwhile, ζ can be estimated experimentally by matching the calculated data with the experimental measures. In addition, in the edge case in which the line width of the metal is equal to its length $l = p$, indicating a hexagon full of metal, FF assumes the value of 1 and the expression R_a coincides with the metal sheet resistance.

Table 4. Aluminum metal grid on ITO: $\tau_g = 80$ nm.

Hexagon Side Length [mm]	Average Sheet Resistance [Ω/\square]	Transmittance at 550 nm [%]
1	5.3 ± 0.4	79
2	7.3 ± 0.6	84
4	10.1 ± 0.9	87
8	10.5 ± 0.9	89

Table 5. Silver metal grid on ITO: $\tau_g = 20$ nm.

Hexagon Side Length [mm]	Average Sheet Resistance [Ω/\square]	Transmittance at 550 nm [%]
1	6.3 ± 0.3	78
2	8.6 ± 0.6	84
4	10.7 ± 0.4	87
8	11.1 ± 0.7	89

While the model is valid for small values of R_a , as illustrated in Figure 16, it loses its significance for low FF , i.e., when l increases. Indeed, in the extreme case where FF tends to zero, R_a would tend to infinity. On the contrary, R_a should tend towards the value of only ITO. For this reason, we are working on the development of a new model that is able to accurately predict the sheet resistance value based on the geometric and physical parameters of the grid.

The electro-optical performance of the two metal grids is also summarized in the graph of $R_a - T_a$ in Figure 17. This graph illustrates that while it would be desirable to have both low resistance and high transmittance, the most feasible approach is to find an optimal

trade-off between these two parameters by adjusting the fill factor and the thickness of the metal grid.

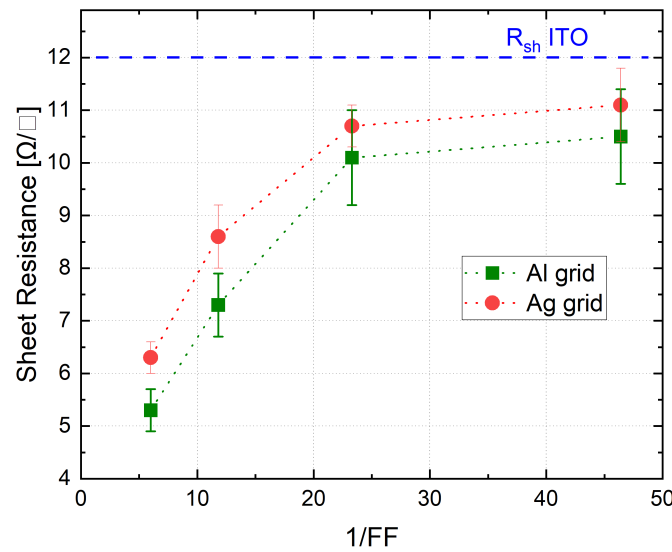


Figure 16. Measured sheet resistance for aluminium and silver grids and reference value for bare ITO.

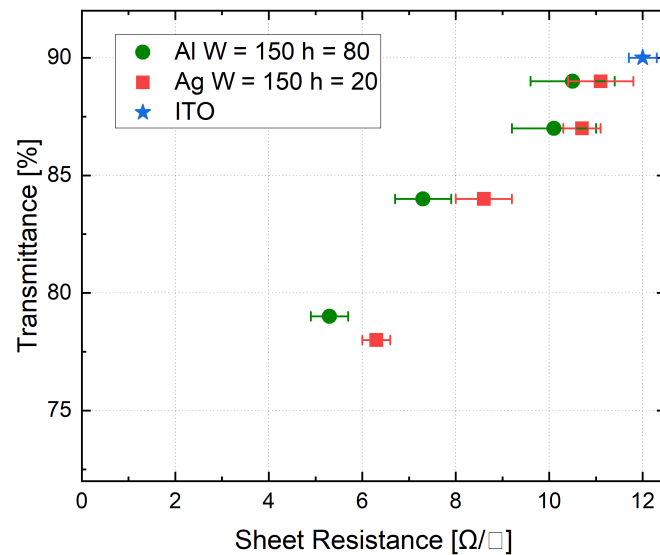


Figure 17. Transmittance plotted as a function of the sheet resistance of the fabricated metal grids on ITO and the reference values for bare ITO. In the legend, h refers to the metal thickness.

The reduced potential drop due to the employment of metal grids in combination with TCO was demonstrated also to lower the Joule heating at the contact, leading to an improvement in the power efficiency and luminosity and an enhancement in the OLED's stability [209]. The contribution of the grid is highlighted by the simulations obtained through finite element modeling, shown in Figure 18, where the characteristics are compared for a $1\text{ cm} \times 1\text{ cm}$ OLED with an ITO electrode and an electrode composed of ITO combined with a metal grid. In particular, the surface potential of the contact, the corresponding current density through the emissive layer, and the dissipated power density are illustrated. The results indicate that for an average current density of 0.5 A/cm^2 , applied at two OLED edges, the surface potential has a voltage drop at the center of the device equal to 600 mV, compared to only 30 mV in the presence of a metal grid. The local current density, evaluated from the potential difference between the top and bottom electrodes, was therefore affected by the variation across the device in the surface potential. In particular, it

showed its maximum at the edges, while, at the center of the pixel, it exhibited a drop of about 15% in the absence of the metal grid and lower than 1.5% with the grid. As a consequence, a significant drop in luminance across the entire surface could occur, especially in the case of larger-sized pixels. The potential gradient also caused an in-plane current associated with the electrode conductance in the ITO region, whereas, in the presence of the grid, this current was concentrated in the metal region and negligible in the ITO area. This current resulted in heat dissipation, as shown in Figure 18, which was concentrated at the pixel edges. However, in the presence of the grid, it was confined to the metal area, resulting in a significant reduction in overall dissipation from 207 mW to only 15 mW thanks to the metal grid.

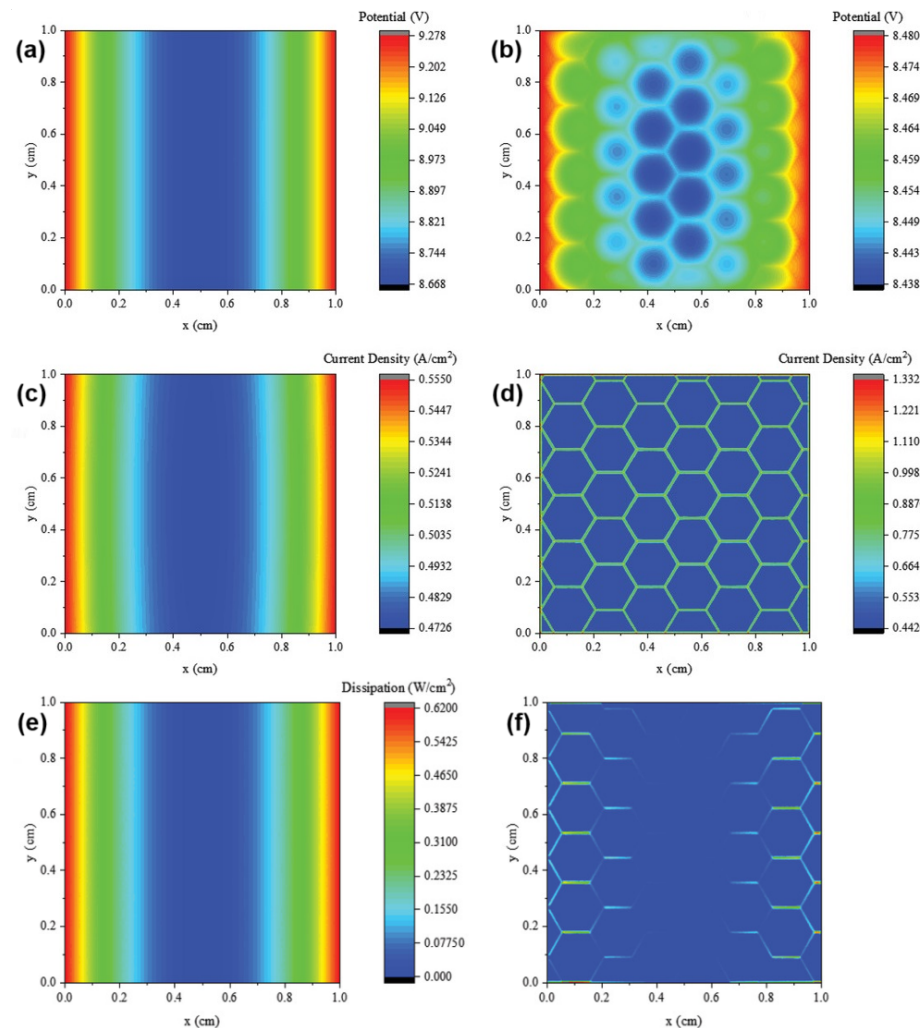


Figure 18. Electrical simulation results for OLED devices consisting of a transparent electrode without or with a metal grid, a thin EML, and a metal electrode. Surface potential of the TCE at an applied voltage corresponding to an average current density of 0.5 A/cm^2 for a TCE based on (a) ITO and (b) ITO/grid. Resulting current density through the EML for a TCE based on (c) ITO and (d) ITO/grid. Dissipated power density for a TCE based on (e) ITO and (f) ITO/grid. Reproduced with permission from [209]. Copyright 2015, John Wiley & Sons–Books.

Metal grids, thanks to the diffusion of consolidated but also emerging solution-based processing techniques [210], are largely employed for flexible substrates and in combination with various TCOs. An example is zinc tin oxide (ZTO), representing a valid indium-free and earth-abundant alternative to ITO. It also stands out due to its low surface roughness ($<0.2 \text{ nm}$), which reduces the probability of device shunting, and due to the high electron mobility of up to $21 \text{ cm}^2/(\text{V s})$. A flexible OLED based on small molecules was success-

fully created with an area of 41 cm², starting from an amorphous ZTO anode deposited by sputtering at a low temperature (60 °C) on a PET substrate, to which a hexagonal molybdenum/aluminum/molybdenum (Mo/Al/Mo) grid was added, followed by the deposition of the organic layers and Al cathode [211]. A photograph of the large-area OLED fabricated on a ZTO/grid anode is reported in Figure 19, where it is shown that its luminance efficiency was greater than that of an OLED deposited on an ITO/grid anode.

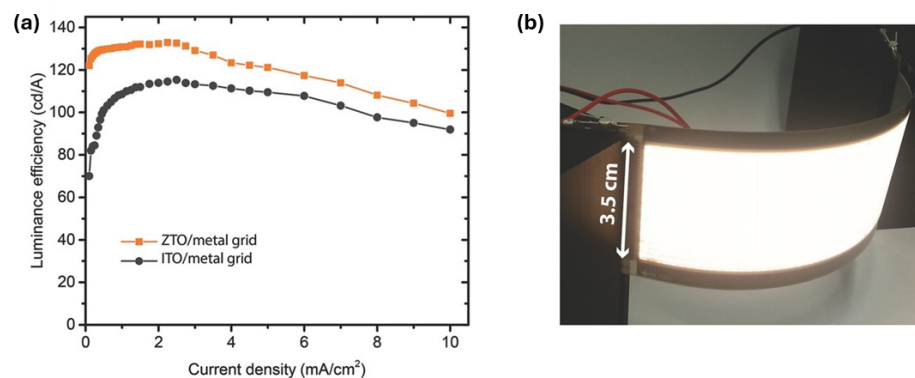


Figure 19. (a) Luminance efficiency as a function of the current density for devices with ZTO/grid and ITO/grid. (b) Photograph of a curved large-area OLED fabricated on a ZTO/grid anode. Reproduced with permission from [211]. Copyright 2015, John Wiley & Sons.

For the production of large-area OLEDs, significant attention has recently been devoted to the roll-to-roll manufacturing technique based on the thermal evaporation of small organic molecules. This methodology, already employed for the production of organic photovoltaic cells [212], is well suited for the industrial-scale fabrication of OLEDs, since it can also contribute to reducing the production times and costs in lighting applications. This process, which generates devices in rolls rather than sheets, is compatible with the materials used to create various types of superior transparent electrodes for OLEDs, such as co-evaporated films. Among these, the Ca:Ag system has been successfully deposited, resulting in films with transmittance of 64% and low sheet resistance of 21 Ω/\square , performance that is comparable to that achieved with standard evaporation on small areas [21].

When the dimensions of the OLED increase, the probability of sudden short circuits rises, irrespective of the applied voltage. This is primarily attributed to particles being embedded in the device area and defects occurring during the fabrication process [213]. These particles within the layers can introduce discontinuities. As the current density intensifies, a very high electric field is generated around these discontinuities, resulting in localized temperature increases and the subsequent disintegration of the films. In more detail, spikes can form, originating from oxide agglomerations during the sputtering process, leading to visible bright spots on the panel. Organic semiconductor dust particles, on the other hand, can generate hot spots, as shown in Figure 20. These defects, especially hot spots, create low-resistance paths between the anode and cathode, easily causing shortening during continuous operation and catastrophic failures [214]. In such cases, ensuring high-quality TCO and adopting careful cleaning practices are possible solutions to mitigate this issue. Other sources of abrupt failure include the presence of metal particles or short circuits in the metal grid, due to mask misalignment or improper patterning during the photolithography phase [215]; these issues can be mitigated through proper etchant preparation, substrate and photomask cleaning, and careful alignment. Similarly, it is crucial to pay attention to the deposition environment and maintain the proper care of all machinery.

Finally, with the aim of improving the emission uniformity in large-area OLEDs, recently, hybrid multilayer electrodes have been designed based on Ag (20 nm)/WO₃/Ag (20 nm)/WO₃, allowing for high electrical conductivity with low optical loss [216]. In particular, this structure managed to provide conductivity similar to that of a single Ag electrode with a thickness of 40 nm, while increasing the external quantum efficiency from

11.5% to 22.5% at 1000 cd/m². This increase is due to the splitting of the thicker silver layer into two half-thickness films, which improves the outcoupling efficiency. Furthermore, when used in the fabrication of an OLED of approximately 57 cm² as a top electrode, it promoted an increase in luminance uniformity from 66% to 77%, showing to be a promising alternative electrode for large-area OLEDs.

The elements that have posed obstacles and the relative possible solutions analyzed for the widespread industrial production of large-area OLEDs are summarized in Figure 21.

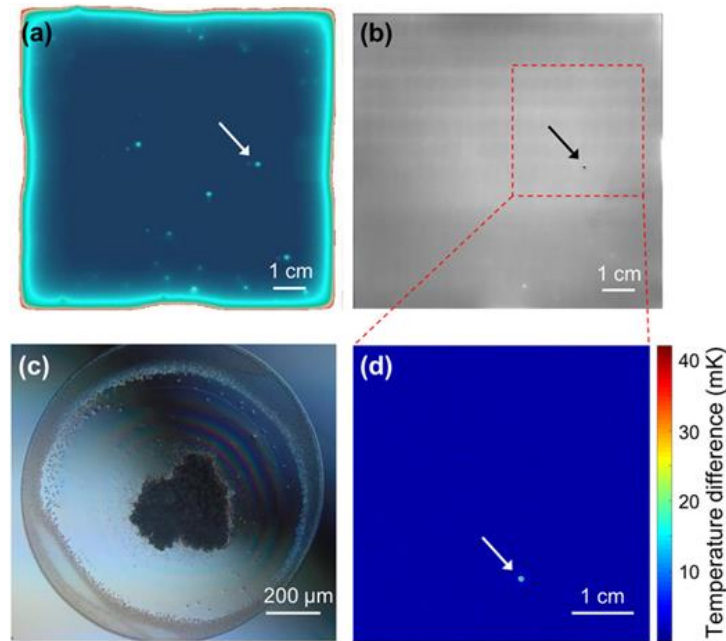


Figure 20. (a) Temperature-selective EL image of a hot spot. (b) EL image showing the formation of a dark spot. (c) Differential interference contrast optical micrograph of the dark spot through the substrate. (d) Thermography image showing the higher temperature surrounding the dark spot. Reproduced with permission from [214]. Copyright 1937, American Institute of Physics.

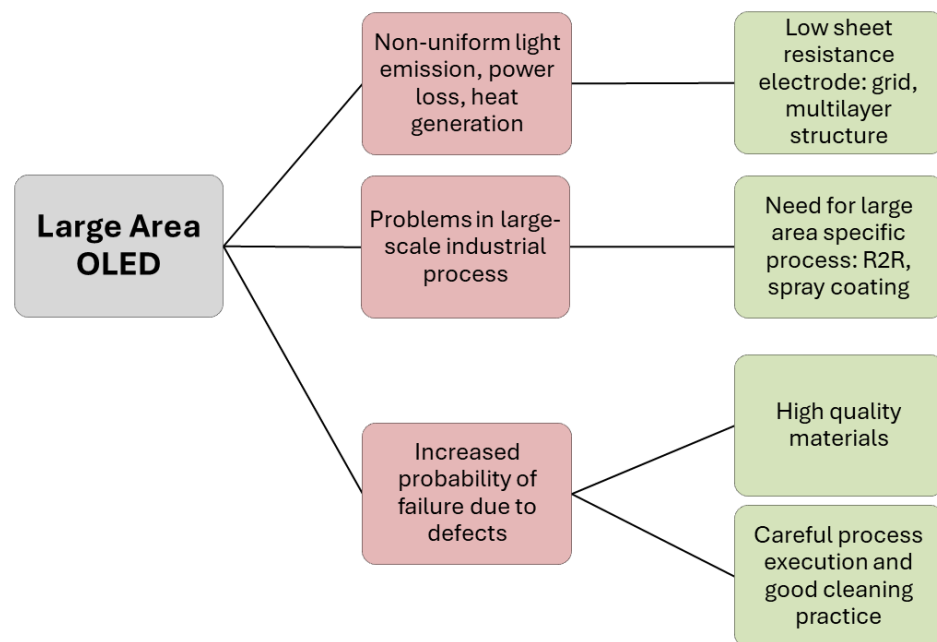


Figure 21. Main issues related to the realization of large-area OLEDs (red boxes) and possible solutions (green boxes) to be adopted.

6. Conclusions

There are several obstacles to overcome to achieve the efficient and cost-effective mass production of OLEDs for lighting applications. It is challenging to simultaneously meet all the requirements that such products demand, including a large area, good efficiency, uniform light emission, a long lifetime, and, in some cases, high transparency and flexibility. Three of the most significant challenges have been reviewed in this paper. White OLEDs require improvements both in terms of materials and optimal layer design. Transparent electrodes necessitate precise control of the deposition processes to obtain enhanced electro-optical properties. In particular, electrodes based on conductive oxides fully meet the transparency requirements but have some limitations due to their deposition processes, which, despite adapting well to large-scale production, can cause damage to the underlying organic materials. To achieve this goal, it is necessary to introduce innovative processes. Thin metals offer a good compromise between conductivity and transparency, especially when employed in DMD structures in combination with an appropriate charge injection layer and an outcoupling layer. In large-area OLEDs, electrodes based on conductive oxides or on thin metal films that are very transparent often exhibit high sheet resistance, causing a voltage drop across the entire OLED area and consequently resulting in non-uniform light distribution. This issue is usually overcome with the use of grids or proper multilayer electrodes. Moreover, in this case, specific manufacturing processes for large areas are needed that are suitable for the industrial context. Significant progress has been made in research with the aim of overcoming these issues, but further improvements are required for OLEDs to become widespread in the future of solid-state lighting, with performance comparable to that of their inorganic counterparts, in different application fields, including smart building lighting, innovative wearables, medical devices, and other consumer products.

Author Contributions: Conceptualization, R.L.; investigation, R.L., F.N. and S.A.; resources, M.G.M.; writing, R.L. and F.N. All authors have read and agreed to the published version of the manuscript.

Funding: This research was funded by RELIGHT project (PON02_00556_3306937) financed by the Ministero dell'Università e della Ricerca (MUR).

Data Availability Statement: Data available on request from the authors.

Conflicts of Interest: The authors declare no conflict of interest.

References

1. Waymouth, J.F. History of Light Sources. In *Handbook of Advanced Lighting Technology*; Karlicek, R., Sun, C.C., Zissis, G., Ma, R., Eds.; Springer International Publishing: Cham, Switzerland, 2017; pp. 3–40. [[CrossRef](#)]
2. Chen, Y.; Ma, D. White OLED Materials. In *Handbook of Advanced Lighting Technology*; Karlicek, R., Sun, C.C., Zissis, G., Ma, R., Eds.; Springer International Publishing: Cham, Switzerland, 2017; pp. 293–320. [[CrossRef](#)]
3. Song, J.; Lee, H.; Jeong, E.G.; Choi, K.C.; Yoo, S. Organic Light-Emitting Diodes: Pushing toward the Limits and Beyond. *Adv. Mater.* **2020**, *32*, 1907539. [[CrossRef](#)]
4. Kido, J.; Hongawa, K.; Okuyama, K.; Nagai, K. White light-emitting organic electroluminescent devices using the poly(N-vinylcarbazole) emitter layer doped with three fluorescent dyes. *Appl. Phys. Lett.* **1994**, *64*, 815–817. [[CrossRef](#)]
5. Wang, Y.Z.; Sun, R.G.; Meghdadi, F.; Leising, G.; Epstein, A.J. Multicolor multilayer light-emitting devices based on pyridine-containing conjugated polymers and para-sexiphenyl oligomer. *Appl. Phys. Lett.* **1999**, *74*, 3613–3615. [[CrossRef](#)]
6. Phelan, G.M. OLED Lighting Hits the Market. *Inf. Disp.* **2018**, *34*, 10–15. [[CrossRef](#)]
7. Liu, S.; Xie, W.; Lee, C.S. Organic light-emitting diodes, what's next? *Next Nanotechnol.* **2023**, *1*, 100003. [[CrossRef](#)]
8. Trivellin, N.; Buffolo, M.; De Santi, C.; Meneghesso, G.; Zanoni, E.; Meneghini, M. Optoelectronic technologies for lighting in automotive: State-of-the-art and perspectives. In Proceedings of the 2023 AEIT International Conference on Electrical and Electronic Technologies for Automotive (AEIT AUTOMOTIVE), Modena, Italy, 17–19 July 2023; pp. 1–6. [[CrossRef](#)]
9. Arneson, C.; Huang, X.; Forrest, S.R. Solid-State Lighting Using Side-by-Side White Phosphorescent Organic Light-Emitting Diodes. *ACS Photonics* **2023**, *10*, 526–533. [[CrossRef](#)]
10. Miller, N.J.; Leon, F.A. *OLED Lighting Products: Capabilities, Challenges, Potential*; Pacific Northwest National Lab. (PNNL): Richland, WA, USA, 2016. [[CrossRef](#)]
11. Kim, T.; Price, J.S.; Grede, A.; Lee, S.; Choi, G.; Guan, W.; Jackson, T.N.; Giebink, N.C. Kirigami-Inspired 3D Organic Light-Emitting Diode (OLED) Lighting Concepts. *Adv. Mater. Technol.* **2018**, *3*, 1800067. [[CrossRef](#)]

12. OLEDWorks—OLED Lighting Installations. Available online: <https://www.oledworks.com/inspiration/> (accessed on 1 December 2023).
13. OLED Light Art Draws Attention to the Theater an der Elbe in Hamburg. Available online: <https://www.ledinside.com/lighting> (accessed on 1 December 2023).
14. May, C.; Toerker, M.; Hesse, J.; Hauptmann, J.; Keibler-Willner, C.; Philipp, A.; Wiczorek, M. 8-3: *Invited Paper: OLED Lighting Design and Roll-to-Roll Manufacturing*. *SID Symp. Dig. Tech. Pap.* **2020**, *51*, 90–92. [[CrossRef](#)]
15. Xu, T.; Zhou, J.G.; Fung, M.K.; Meng, H. Simplified efficient warm white tandem organic light-emitting devices by ultrathin emitters using energy transfer from exciplexes. *Org. Electron.* **2018**, *63*, 369–375. [[CrossRef](#)]
16. Avci, A.N.; Akbay, S. A Review based on OLED Lighting Conditions and Human Circadian System. *Cult. E Sci. Del Colore-Color Cult. Sci.* **2023**, *15*, 7–12. [[CrossRef](#)]
17. Imbrasas, P.; Lenk, S.; Reineke, S. Organic light-emitting diodes with split recombination zones: A concept for versatile color tuning. *Org. Electron.* **2020**, *78*, 105558. [[CrossRef](#)]
18. Li, Y.; Liu, N.; Zhou, P.; Lan, W.; Pu, H.; Liao, Y. Efficient and Color-tunable Organic Light-emitting Diodes for Rear Light Application on the Motor Vehicle. *Mater. Sci.* **2021**, *27*, 264–268. [[CrossRef](#)]
19. Migliaccio, L.; Aprano, S.; Iannuzzi, L.; Maglione, M.G.; Tassini, P.; Minarini, C.; Manini, P.; Pezzella, A. Eumelanin–PEDOT:PSS Complementing En Route to Mammalian-Pigment-Based Electrodes: Design and Fabrication of an ITO-Free Organic Light-Emitting Device. *Adv. Electron. Mater.* **2017**, *3*, 1600342. [[CrossRef](#)]
20. Manini, P.; Criscuolo, V.; Ricciotti, L.; Pezzella, A.; Barra, M.; Cassinese, A.; Crescenzi, O.; Maglione, M.G.; Tassini, P.; Minarini, C.; et al. Melanin-Inspired Organic Electronics: Electroluminescence in Asymmetric Triazatruxenes. *ChemPlusChem* **2015**, *80*, 898. [[CrossRef](#)] [[PubMed](#)]
21. Wang, D.; Hauptmann, J.; May, C.; Hofstetter, Y.J.; Vaynzof, Y.; Müller, T. Roll-to-roll fabrication of highly transparent Ca:Ag top-electrode towards flexible large-area OLED lighting application. *Flex. Print. Electron.* **2021**, *6*, 035001. [[CrossRef](#)]
22. Pode, R.; Diouf, B. *OLED Lighting Technology*. In *Solar Lighting*; Springer: London, UK, 2011; pp. 97–149. [[CrossRef](#)]
23. Reineke, S.; Thomschke, M.; Lüssem, B.; Leo, K. White organic light-emitting diodes: Status and perspective. *Rev. Mod. Phys.* **2013**, *85*, 1245. [[CrossRef](#)]
24. Ma, D. White OLED Devices. In *Handbook of Advanced Lighting Technology*; Karlicek, R., Sun, C.C., Zissis, G., Ma, R., Eds.; Springer International Publishing: Cham, Switzerland, 2017; pp. 321–361. [[CrossRef](#)]
25. Huseynova, G.; Lee, J.; Kim, Y.H.; Lee, J. Transparent Organic Light-Emitting Diodes: Advances, Prospects, and Challenges. *Adv. Opt. Mater.* **2021**, *9*, 2002040. [[CrossRef](#)]
26. Fiorillo, M.; Rubino, A.; Santoro, E.; Maglione, M.; Minarini, C.; Aprano, S.; Tassini, P.; Sico, G. *Evaluation of the Stability of Different Encapsulated Blue OLEDs*; Institution of Engineering and Technology: Turin, Italy, 2015; pp. 1–4. [[CrossRef](#)]
27. Swayamprabha, S.S.; Dubey, D.K.; Shahnawaz; Yadav, R.A.K.; Nagar, M.R.; Sharma, A.; Tung, F.; Jou, J. Approaches for Long Lifetime Organic Light Emitting Diodes. *Adv. Sci.* **2021**, *8*, 2254. [[CrossRef](#)]
28. Jeon, Y.; Lee, H.; Kim, H.; Kwon, J.H. A Review of Various Attempts on Multi-Functional Encapsulation Technologies for the Reliability of OLEDs. *Micromachines* **2022**, *13*, 1478. [[CrossRef](#)]
29. Ramasamy, E.; Karthikeyan, V.; Rameshkumar, K.; Veerappan, G. Glass-to-glass encapsulation with ultraviolet light curable epoxy edge sealing for stable perovskite solar cells. *Mater. Lett.* **2019**, *250*, 51–54. [[CrossRef](#)]
30. Spindler, J.; Kondakova, M.; Boroson, M.; Büchel, M.; Eser, J.; Knipping, J. 84-1: *Invited Paper: Advances in High Efficacy and Flexible OLED Lighting*. *SID Symp. Dig. Tech. Pap.* **2018**, *49*, 1135–1138. [[CrossRef](#)]
31. Nowy, S.; Krummacher, B.C.; Frischeisen, J.; Reinke, N.A.; Brütting, W. Light extraction and optical loss mechanisms in organic light-emitting diodes: Influence of the emitter quantum efficiency. *J. Appl. Phys.* **2008**, *104*, 123109. [[CrossRef](#)]
32. Kim, J.Y.; Joo, C.W.; Lee, J.; Woo, J.C.; Oh, J.Y.; Baek, N.S.; Chu, H.Y.; Lee, J.I. Save energy on OLED lighting by a simple yet powerful technique. *RSC Adv.* **2015**, *5*, 8415–8421. [[CrossRef](#)]
33. Zhou, R.; Chung, H.S.H.; Zhang, R. An Inductive Power Transfer System for Driving Multiple OLED Light Panels. *IEEE Trans. Power Electron.* **2016**, *31*, 7131–7147. [[CrossRef](#)]
34. Bender, V.C.; Barth, N.D.; Mendes, F.B.; Pinto, R.A.; Alonso, J.M.; Marchesan, T.B. A Hardware Emulator for OLED Panels Applied to Lighting Systems. *IEEE J. Emerg. Sel. Top. Power Electron.* **2018**, *6*, 1252–1258. [[CrossRef](#)]
35. Lu, M.M.; Ngai, P. OLED Requirements for Solid-State Lighting. *Inf. Disp.* **2010**, *26*, 10–13. [[CrossRef](#)]
36. Forrest, S.; Bradley, D.; Thompson, M. Measuring the Efficiency of Organic Light-Emitting Devices. *Adv. Mater.* **2003**, *15*, 1043–1048. [[CrossRef](#)]
37. Liu, Y.; Ding, T.; Chen, X.; Bai, F.; Genco, A.; Wang, H.; Chen, C.; Chen, P.; Mazzeo, M.; Zhang, Y.; et al. Highly Conductive Alkaline-Earth Metal Electrodes: The Possibility of Maintaining Both Low Work Function and Surface Stability for Organic Electronics. *Adv. Opt. Mater.* **2020**, *8*, 2000206. [[CrossRef](#)]
38. Pode, R. Organic light emitting diode devices: An energy efficient solid state lighting for applications. *Renew. Sustain. Energy Rev.* **2020**, *133*, 110043. [[CrossRef](#)]
39. Thejokalyani, N.; Dhoble, S. Importance of Eco-Friendly OLED Lighting. *Defect Diffus. Forum* **2014**, *357*, 1–27. [[CrossRef](#)]
40. Kang, J.; Cho, Y.; Jang, W. Long-Term Reliability Characteristics of OLED Panel and Luminaires for General Lighting Applications. *Appl. Sci.* **2020**, *11*, 74. [[CrossRef](#)]

41. Liu, H.; Liu, F.; Lu, P. Multiple strategies towards high-efficiency white organic light-emitting diodes by the vacuum deposition method. *J. Mater. Chem. C* **2020**, *8*, 5636–5661. [[CrossRef](#)]
42. Chowdhury, D.Q.; Garner, S.M.; Lewis, S.C. Application of OLED for Automotive Lighting. In Proceedings of the 2019 26th International Workshop on Active-Matrix Flatpanel Displays and Devices (AM-FPD), Kyoto, Japan, 2–5 July 2019; pp. 1–3. [[CrossRef](#)]
43. Zou, S.J.; Shen, Y.; Xie, F.M.; Chen, J.D.; Li, Y.Q.; Tang, J.X. Recent advances in organic light-emitting diodes: Toward smart lighting and displays. *Mater. Chem. Front.* **2020**, *4*, 788–820. [[CrossRef](#)]
44. Duggal, A.R.; Shiang, J.J.; Foust, D.F.; Turner, L.G.; Nealon, W.F.; Bortscheller, J.C. 4.1: Invited Paper: Large Area White OLEDs. *SID Symp. Dig. Tech. Pap.* **2005**, *36*, 28–31. [[CrossRef](#)]
45. ORBEOSTM for OLED Lighting. Available online: <https://www.mouser.it/datasheet/2/588/cdw031orbeos-2891335.pdf> (accessed on 1 December 2023).
46. OLED-Info: The OLED Experts. Available online: <https://www.oled-info.com/> (accessed on 1 December 2023).
47. Komoda, T.; Tsuji, H.; Ito, N.; Nishimori, T.; Ide, N. 66.4: Invited Paper: High-Quality White OLEDs and Resource Saving Fabrication Processes for Lighting Application. *SID Symp. Dig. Tech. Pap.* **2010**, *41*, 993–996. [[CrossRef](#)]
48. Verbatim. Available online: <https://www.verbatim.com/index/newsroom.php> (accessed on 1 December 2023).
49. Levermore, P.A.; Adamovich, V.; Rajan, K.; Yeager, W.; Lin, C.; Xia, S.; Kottas, G.S.; Weaver, M.S.; Kwong, R.; Ma, R.; et al. 52.4: Highly Efficient Phosphorescent OLED Lighting Panels for Solid State Lighting. *SID Symp. Dig. Tech. Pap.* **2010**, *41*, 786–789. [[CrossRef](#)]
50. Tsujimura, T. OLED Lighting. In *OLED Display Fundamentals and Applications*; John Wiley & Sons, Ltd.: Hoboken, NJ, USA, 2017; Chapter 9, pp. 255–276. [[CrossRef](#)]
51. Jang, S.; Lee, Y.; Park, M. 44.1: Invited Paper: OLED Lighting for General Lighting Applications. *SID Symp. Dig. Tech. Pap.* **2015**, *46*, 661–663. [[CrossRef](#)]
52. Spindler, J.; Kondakova, M.; Boroson, M.; Hamer, J.; Gohri, V.; Büchel, M.; Ruske, M.; Meulancamp, E. 24-2: Invited Paper: High Brightness OLED Lighting. *SID Symp. Dig. Tech. Pap.* **2016**, *47*, 294–297. [[CrossRef](#)]
53. Cooper, G.D.; Monickam, S. 84-2: Invited Paper: High Refractive Index Light Extraction for OLED Lighting. *SID Symp. Dig. Tech. Pap.* **2018**, *49*, 1139–1142. [[CrossRef](#)]
54. Kim, H.; Shin, H.; Park, J.; Choi, Y.; Park, J. Statistical modeling and reliability prediction for transient luminance degradation of flexible OLEDs. In Proceedings of the 2018 IEEE International Reliability Physics Symposium (IRPS), Burlingame, CA, USA, 11–15 March 2018; pp. 3C.7–1–3C.7–6. [[CrossRef](#)]
55. Alchaddoud, A.; Canale, L.; Ibrahim, G.; Zissis, G. Photometric and Electrical Characterizations of Large-Area OLEDs Aged Under Thermal and Electrical Stresses. *IEEE Trans. Ind. Appl.* **2019**, *55*, 991–995. [[CrossRef](#)]
56. Salameh, F.; Al Haddad, A.; Picot, A.; Canale, L.; Zissis, G.; Chabert, M.; Maussion, P. Modeling the Luminance Degradation of OLEDs Using Design of Experiments. *IEEE Trans. Ind. Appl.* **2019**, *55*, 6548–6558. [[CrossRef](#)]
57. IEC 62922:2016/AMD1:2021 ED1. Available online: https://www.iec.ch/dyn/www/?p=103:38:14509173073973:::FSP_ORG_ID,FSP_APEX_PAGE,FSP_PROJECT_ID:1340,23,101920 (accessed on 1 December 2023).
58. Yeom, J.M.; Jung, H.J.; Choi, S.Y.; Lee, D.S.; Lim, S.R. Environmental effects of the technology transition from liquid—Crystal display (LCD) to organic light-emitting diode (OLED) display from an e-waste management perspective. *Int. J. Environ. Res.* **2018**, *12*, 479–488. [[CrossRef](#)]
59. Cocchi, M.; Bertoldo, M.; Seri, M.; Maccagnani, P.; Summonte, C.; Buoso, S.; Belletti, G.; Dinelli, F.; Capelli, R. Fully Recyclable OLEDs Built on a Flexible Biopolymer Substrate. *ACS Sustain. Chem. Eng.* **2021**, *9*, 12733–12737. [[CrossRef](#)]
60. Hanif, A. Sustainable use of organic light-emitting diode (OLED) and liquid crystal display (LCD) glass wastes as cement replacement in concrete. *Mater. Today Proc.* **2023**, *in press*. [[CrossRef](#)]
61. Le Rendu, P.; Nguyen, T.; Carrois, L. Cellulose acetate and PVDC used as protective layers for organic diodes. *Synth. Met.* **2003**, *138*, 285–288. [[CrossRef](#)]
62. Najafabadi, E.; Zhou, Y.H.; Knauer, K.A.; Fuentes-Hernandez, C.; Kippelen, B. Efficient organic light-emitting diodes fabricated on cellulose nanocrystal substrates. *Appl. Phys. Lett.* **2014**, *105*, 063305. [[CrossRef](#)]
63. Dong, H.; Wu, Z.; Jiang, Y.; Liu, W.; Li, X.; Jiao, B.; Abbas, W.; Hou, X. A Flexible and Thin Graphene/Silver Nanowires/Polymer Hybrid Transparent Electrode for Optoelectronic Devices. *ACS Appl. Mater. Interfaces* **2016**, *8*, 31212–31221. [[CrossRef](#)] [[PubMed](#)]
64. Liu, Y.; Xie, Y.; Liu, Y.; Song, T.; Zhang, K.Q.; Liao, L.; Sun, B. Flexible organic light emitting diodes fabricated on biocompatible silk fibroin substrate. *Semicond. Sci. Technol.* **2015**, *30*, 104004. [[CrossRef](#)]
65. Hendler, N.; Wildeman, J.; Mentovich, E.D.; Schnitzler, T.; Belgorodsky, B.; Prusty, D.K.; Rimmerman, D.; Herrmann, A.; Richter, S. Efficient Separation of Conjugated Polymers Using a Water Soluble Glycoprotein Matrix: From Fluorescence Materials to Light Emitting Devices. *Macromol. Biosci.* **2014**, *14*, 320–326. [[CrossRef](#)] [[PubMed](#)]
66. Gomez, E.F.; Venkatraman, V.; Grote, J.G.; Steckl, A.J. DNA bases thymine and adenine in bio-organic light emitting diodes. *Sci. Rep.* **2014**, *4*, 7105. [[CrossRef](#)] [[PubMed](#)]
67. Gomez, E.F.; Venkatraman, V.; Grote, J.G.; Steckl, A.J. Exploring the Potential of Nucleic Acid Bases in Organic Light Emitting Diodes. *Adv. Mater.* **2015**, *27*, 7552–7562. [[CrossRef](#)] [[PubMed](#)]

68. Jürgensen, N.; Ackermann, M.; Marszalek, T.; Zimmermann, J.; Morfa, A.J.; Pisula, W.; Bunz, U.H.F.; Hinkel, F.; Hernandez-Sosa, G. Solution-Processed Bio-OLEDs with a Vitamin-Derived Riboflavin Tetrabutryrate Emission Layer. *ACS Sustain. Chem. Eng.* **2017**, *5*, 5368–5372. [[CrossRef](#)]
69. Nakamura, K.; Minami, H.; Sagara, A.; Itamoto, N.; Kobayashi, N. Enhanced red emissions of europium(III) chelates in DNA–CTMA complexes. *J. Mater. Chem. C* **2018**, *6*, 4516–4522. [[CrossRef](#)]
70. Zissis, G.; Bertoldi, P.; Serrenho, T. *Update on the Status of LED-Lighting World Market Since 2018*; Publications Office of the European Union: Luxembourg, 2021. [[CrossRef](#)]
71. Forrest, S.R. *From Deposition to Encapsulation: Roll-to-Roll Manufacturing of Organic Light Emitting Devices for Lighting (Final Report)*; University of Michigan: Ann Arbor, MI, USA, 2023. [[CrossRef](#)]
72. Qu, B.; Chen, Z.; Lahann, L.; Forrest, S.R. Cost Estimates of Roll-to-Roll Production of Organic Light Emitting Devices for Lighting. *ACS Photonics* **2023**, *10*, 1850–1858. [[CrossRef](#)]
73. Gather, M.C.; Köhnen, A.; Meerholz, K. White Organic Light-Emitting Diodes. *Adv. Mater.* **2011**, *23*, 233–248. [[CrossRef](#)] [[PubMed](#)]
74. Rippa, M.; Capasso, R.; Petti, L.; Nenna, G.; Mauro, A.D.G.D.; Maglione, M.G.; della Noce, M.; Minarini, C. Photonic quasi crystals to enhance light extraction efficiency for White OLEDs applications. In Proceedings of the 2014 Fotonica AEIT Italian Conference on Photonics Technologies, Naples, Italy, 12–14 May 2014; pp. 1–4. [[CrossRef](#)]
75. Rippa, M.; Capasso, R.; Petti, L.; Nenna, G.; Mauro, A.D.G.D.; Maglione, M.G.; Minarini, C. Nanostructured PEDOT:PSS film with two-dimensional photonic quasi crystals for efficient white OLED devices. *J. Mater. Chem. C* **2015**, *3*, 147–152. [[CrossRef](#)]
76. Liguori, R.; Sheets, W.; Facchetti, A.; Rubino, A. Light- and bias-induced effects in pentacene-based thin film phototransistors with a photocurable polymer dielectric. *Org. Electron.* **2016**, *28*, 147–154. [[CrossRef](#)]
77. Liguori, R.; Usta, H.; Fusco, S.; Facchetti, A.; Licciardo, G.D.; Benedetto, L.D.; Rubino, A. Insights Into Interface Treatments in p-Channel Organic Thin-Film Transistors Based on a Novel Molecular Semiconductor. *IEEE Trans. Electron Devices* **2017**, *64*, 2338–2344. [[CrossRef](#)]
78. Xiao, L.; Chen, Z.; Qu, B.; Luo, J.; Kong, S.; Gong, Q.; Kido, J. Recent Progresses on Materials for Electrophosphorescent Organic Light-Emitting Devices. *Adv. Mater.* **2011**, *23*, 926–952. [[CrossRef](#)] [[PubMed](#)]
79. Turner, E.; Bakken, N.; Li, J. Cyclometalated Platinum Complexes with Luminescent Quantum Yields Approaching 100%. *Inorg. Chem.* **2013**, *52*, 7344–7351. [[CrossRef](#)] [[PubMed](#)]
80. Xue, C.; Lin, H.; Zhang, G.; Hu, Y.; Jiang, W.; Lang, J.; Wang, D.; Xing, G. Recent advances in thermally activated delayed fluorescence for white OLEDs applications. *J. Mater. Sci. Mater. Electron.* **2020**, *31*, 4444–4462. [[CrossRef](#)]
81. Liu, F.; Liu, H.; Tang, X.; Ren, S.; He, X.; Li, J.; Du, C.; Feng, Z.; Lu, P. Novel blue fluorescent materials for high-performance nondoped blue OLEDs and hybrid pure white OLEDs with ultrahigh color rendering index. *Nano Energy* **2020**, *68*, 104325. [[CrossRef](#)]
82. Zhang, K.; Zhang, W.; Cao, Q.; Zhou, T.; Ge, F.; Xu, H.; Wang, J.; Ban, X.; Zhang, T. Turning the energy channel of side-chain TADF polymers by monomer optimization for high-efficiency solution-processed white OLEDs. *J. Lumin.* **2023**, *263*, 119966. [[CrossRef](#)]
83. Gärditz, C.; Paetzold, R.; Buchhauser, D.; Bathelt, R.; Gieres, G.; Tschamber, C.; Hunze, A.; Heuser, K.; Winnacker, A.; Amelung, J.; et al. OLED lighting based on white broadband copolymer emitters. In Proceedings of the Volume 5937, Organic Light-Emitting Materials and Devices IX, San Diego, CA, USA, 31 July–4 August 2005; p. 59370L. [[CrossRef](#)]
84. Gioti, M.; Kokkinos, D.; Stavrou, K.; Simitzi, K.; Andreopoulou, A.; Laskarakis, A.; Kallitsis, J.; Logothetidis, S. Fabrication and Study of White-Light OLEDs Based on Novel Copolymers with Blue, Yellow, and Red Chromophores. *Phys. Status Solidi (RRL)—Rapid Res. Lett.* **2019**, *13*, 1800419. [[CrossRef](#)]
85. Tselekidou, D.; Papadopoulos, K.; Kyriazopoulos, V.; Andrikopoulos, K.C.; Andreopoulou, A.K.; Kallitsis, J.K.; Laskarakis, A.; Logothetidis, S.; Gioti, M. Photophysical and Electro-Optical Properties of Copolymers Bearing Blue and Red Chromophores for Single-Layer White OLEDs. *Nanomaterials* **2021**, *11*, 2629. [[CrossRef](#)] [[PubMed](#)]
86. Ban, X.; Chen, F.; Pan, J.; Liu, Y.; Zhu, A.; Jiang, W.; Sun, Y. Exciplex Formation and Electromer Blocking for Highly Efficient Blue Thermally Activated Delayed Fluorescence OLEDs with All-Solution-Processed Organic Layers. *Chem.—A Eur. J.* **2020**, *26*, 3090–3102. [[CrossRef](#)]
87. Chang, Y.C.; Chang, J.Y.; Liou, B.T.; Huang, M.F.; Kuo, Y.K. Effect of exciton-blocking layer on the characteristics of multilayer white organic light-emitting diodes. In Proceedings of the Volume 11683, Organic Photonic Materials and Devices XXIII, SPIE, Online, 6–12 March 2021; p. 33. [[CrossRef](#)]
88. Miao, Y.; Zhao, B.; Gao, Z.; Shi, H.; Tao, P.; Wu, Y.; Wang, K.; Wang, H.; Xu, B.; Zhu, F. A novel intramolecular charge transfer blue fluorophor for high color stability hybrid di-chromatic white organic light-emitting diodes. *Org. Electron.* **2017**, *42*, 1–7. [[CrossRef](#)]
89. Yang, H.; Peng, X.; Cao, C.; Wu, L.; Chen, N.; Zhang, X.; Xie, W.; Tong, Q.; Wu, Z. A deep blue fluorescent emitter functioning as host material in highly efficient phosphorescent and hybrid white organic light-emitting devices. *Org. Electron.* **2020**, *85*, 105848. [[CrossRef](#)]
90. Sun, Y.; Giebink, N.C.; Kanno, H.; Ma, B.; Thompson, M.E.; Forrest, S.R. Management of singlet and triplet excitons for efficient white organic light-emitting devices. *Nature* **2006**, *440*, 908–912. [[CrossRef](#)]
91. Schwartz, G.; Pfeiffer, M.; Reineke, S.; Walzer, K.; Leo, K. Harvesting Triplet Excitons from Fluorescent Blue Emitters in White Organic Light-Emitting Diodes. *Adv. Mater.* **2007**, *19*, 3672–3676. [[CrossRef](#)]

92. Hofmann, S.; Furno, M.; Lüsse, B.; Leo, K.; Gather, M.C. Investigation of triplet harvesting and outcoupling efficiency in highly efficient two-color hybrid white organic light-emitting diodes. *Phys. Status Solidi (A)* **2013**, *210*, 1467–1475. [[CrossRef](#)]
93. Ren, Q.; Zhao, Y.; Liu, C.; Zhan, H.; Cheng, Y.; Li, W. Efficient triplet harvest for orange-red and white OLEDs based exciplex host with different donor/acceptor ratios. *Opt. Mater.* **2021**, *113*, 110907. [[CrossRef](#)]
94. Chen, S.; Kwok, H.S. Top-emitting white organic light-emitting diodes with a color conversion cap layer. *Org. Electron.* **2011**, *12*, 677–681. [[CrossRef](#)]
95. Jo, D.S.; Dang, T.M.L.; Tran, T.T.; Kim, M.J.; Chung, H.K.; Jung, S.; Cho, S.M.; Chae, H.; Yoon, D.H. Fabrication of color conversion layers using adhesive transfer of phosphor particles for improving light extraction efficiency and uniformity of down-conversion white OLED. *Opt. Mater.* **2021**, *114*, 110772. [[CrossRef](#)]
96. Botta, A.; Pragliola, S.; Venditto, V.; Rubino, A.; Aprano, S.; Mauro, A.D.G.D.; Maglione, M.G.; Minarini, C. Synthesis, characterization, and use as emissive layer of white organic light emitting diodes of the highly isotactic poly(*N*-pentenyl-carbazole). *Polym. Compos.* **2015**, *36*, 1110–1117. [[CrossRef](#)]
97. Botta, A.; Pragliola, S.; Capacchione, C.; Rubino, A.; Liguori, R.; Mauro, A.D.G.D.; Venditto, V. Synthesis of poly(4-(*N*-carbazolyl)methyl styrene)s: Tailoring optical properties through stereoregularity. *Eur. Polym. J.* **2017**, *88*, 246–256. [[CrossRef](#)]
98. Liguori, R.; Botta, A.; Pragliola, S.; Rubino, A.; Venditto, V.; Velardo, A.; Aprano, S.; Maglione, M.G.; Prontera, C.T.; Mauro, A.D.G.D.; et al. Study of the electroluminescence of highly stereoregular poly(*N*-pentenyl-carbazole) for blue and white OLEDs. *Semicond. Sci. Technol.* **2017**, *32*, 065006. [[CrossRef](#)]
99. Botta, A.; Costabile, C.; Venditto, V.; Pragliola, S.; Liguori, R.; Rubino, A.; Alberga, D.; Savarese, M.; Adamo, C. Optoelectronic properties of poly(*N*-alkenyl-carbazole)s driven by polymer stereoregularity. *J. Polym. Sci. Part A Polym. Chem.* **2018**, *56*, 242–251. [[CrossRef](#)]
100. Liguori, R.; Rubino, A.; Botta, A.; Pragliola, S. Blue and white OLEDs with highly stereoregular polymers. In Proceedings of the 2017 International Semiconductor Conference (CAS), Sinaia, Romania, 11–14 October 2017; pp. 79–82. [[CrossRef](#)]
101. Liguori, R.; Botta, A.; Rubino, A.; Pragliola, S.; Venditto, V. Stereoregular polymers with pendant carbazolyl groups: Synthesis, properties and optoelectronic applications. *Synth. Met.* **2018**, *246*, 185–194. [[CrossRef](#)]
102. Jou, J.H.; Chen, P.W.; Chen, Y.L.; Jou, Y.C.; Tseng, J.R.; Wu, R.Z.; Hsieh, C.Y.; Hsieh, Y.C.; Joers, P.; Chen, S.H.; et al. OLEDs with chromaticity tunable between dusk-hue and candle-light. *Org. Electron.* **2013**, *14*, 47–54. [[CrossRef](#)]
103. Spindler, J. *Mask Free OLED Fabrication Process for Non-Tunable and Tunable White OLED Panels*; OLEDWorks LLC: Rochester, NY, USA, 2021. [[CrossRef](#)]
104. Zhao, Y.; Chen, R.; Gao, Y.; Leck, K.S.; Yang, X.; Liu, S.; Abiyasa, A.P.; Divayana, Y.; Mutlugun, E.; Tan, S.T.; et al. AC-driven, color- and brightness-tunable organic light-emitting diodes constructed from an electron only device. *Org. Electron.* **2013**, *14*, 3195–3200. [[CrossRef](#)]
105. Chen, Z.; Ho, C.; Wang, L.; Wong, W. Single-Molecular White-Light Emitters and Their Potential WOLED Applications. *Adv. Mater.* **2020**, *32*, 1903269. [[CrossRef](#)] [[PubMed](#)]
106. Huang, C.W.; Lin, T.A.; Lee, W.K.; Lu, C.H.; Chatterjee, T.; Chou, C.H.; Wong, K.T.; Wu, C.C. Analyses of emission efficiencies of white organic light-emitting diodes having multiple emitters in single emitting layer. *Org. Electron.* **2022**, *104*, 106474. [[CrossRef](#)]
107. Chang, Y.; Ren, Q.; Zhang, R.; Zhao, Y.; Wang, H. A low cost and simple structured WOLED device based on exciplex host and full fluorescent materials. *Solid-State Electron.* **2023**, *208*, 108753. [[CrossRef](#)]
108. Ameri, L.; Cao, L.; Tan, X.; Li, J. Efficient, Color-Stable, and Long-Lived White Organic Light-Emitting Diodes Utilizing Phosphorescent Molecular Aggregates. *Adv. Mater.* **2023**, *35*, 2208361. [[CrossRef](#)] [[PubMed](#)]
109. Wang, T.H.; Yi, L.B.; Chu, S.Y.; Kao, P.C. High-performance warm-white OLEDs using interfacial exciplex energy transfer with external quantum efficiency exceeding 30%. *Synth. Met.* **2024**, *301*, 117530. [[CrossRef](#)]
110. Cao, W.; Li, J.; Chen, H.; Xue, J. Transparent electrodes for organic optoelectronic devices: A review. *J. Photonics Energy* **2014**, *4*, 040990. [[CrossRef](#)]
111. Huseynova, G.; Kim, Y.H.; Lee, J.H.; Lee, J. Emission characteristics of transparent organic light-emitting diodes with molybdenum oxide capping layers. *Synth. Met.* **2020**, *262*, 116335. [[CrossRef](#)]
112. Tian, Y.; Wang, T.; Zhu, Q.; Zhang, X.; Ethiraj, A.S.; Geng, W.M.; Geng, H.Z. High-Performance Transparent PEDOT: PSS/CNT Films for OLEDs. *Nanomaterials* **2021**, *11*, 2067. [[CrossRef](#)] [[PubMed](#)]
113. Sharma, S.; Shriwastava, S.; Kumar, S.; Bhatt, K.; Tripathi, C.C. Alternative transparent conducting electrode materials for flexible optoelectronic devices. *Opto-Electron. Rev.* **2018**, *26*, 223–235. [[CrossRef](#)]
114. Zeng, X.Y.; Tang, Y.Q.; Cai, X.Y.; Tang, J.X.; Li, Y.Q. Solution-processed OLEDs for printing displays. *Mater. Chem. Front.* **2023**, *7*, 1166–1196. [[CrossRef](#)]
115. Woo, Y. Transparent Conductive Electrodes Based on Graphene-Related Materials. *Micromachines* **2018**, *10*, 13. [[CrossRef](#)] [[PubMed](#)]
116. Adetayo, A.E.; Ahmed, T.N.; Zakhidov, A.; Beall, G.W. Improvements of Organic Light-Emitting Diodes Using Graphene as an Emerging and Efficient Transparent Conducting Electrode Material. *Adv. Opt. Mater.* **2021**, *9*, 2002102. [[CrossRef](#)]
117. Shi, D.; Resasco, D.E. Study of the growth of conductive single-wall carbon nanotube films with ultra-high transparency. *Chem. Phys. Lett.* **2011**, *511*, 356–362. [[CrossRef](#)]

118. Seo, T.H.; Lee, S.; Min, K.H.; Chandramohan, S.; Park, A.H.; Lee, G.H.; Park, M.; Suh, E.K.; Kim, M.J. The role of graphene formed on silver nanowire transparent conductive electrode in ultra-violet light emitting diodes. *Sci. Rep.* **2016**, *6*, 29464. [[CrossRef](#)] [[PubMed](#)]
119. Choo, D.C.; Kim, T.W. Degradation mechanisms of silver nanowire electrodes under ultraviolet irradiation and heat treatment. *Sci. Rep.* **2017**, *7*, 1696. [[CrossRef](#)] [[PubMed](#)]
120. Celle, C.; Cabos, A.; Fontecave, T.; Laguitton, B.; Benayad, A.; Guettaz, L.; Pélissier, N.; Nguyen, V.H.; Bellet, D.; Muñoz-Rojas, D.; et al. Oxidation of copper nanowire based transparent electrodes in ambient conditions and their stabilization by encapsulation: Application to transparent film heaters. *Nanotechnology* **2018**, *29*, 085701. [[CrossRef](#)] [[PubMed](#)]
121. Hadjab, M.; Guskova, O.; Bennacer, H.; Ziane, M.I.; Larbi, A.H.; Saeed, M. Ground-state properties of p-type delafossite transparent conducting oxides 2H-CuMO₂ (M = Al, Sc and Y): DFT calculations. *Mater. Today Commun.* **2022**, *32*, 103995. [[CrossRef](#)]
122. Blair, S.F.J.; Male, J.S.; Cavill, S.A.; Reardon, C.P.; Krauss, T.F. Photonic Characterisation of Indium Tin Oxide as a Function of Deposition Conditions. *Nanomaterials* **2023**, *13*, 1990. [[CrossRef](#)]
123. Wang, K.; Jiao, P.; Cheng, Y.; Xu, H.; Zhu, G.; Zhao, Y.; Jiang, K.; Zhang, X.; Su, Y. ITO films with different preferred orientations prepared by DC magnetron sputtering. *Opt. Mater.* **2022**, *134*, 113040. [[CrossRef](#)]
124. Li, H.; Ruan, C.; Sun, Q.; Rui, M.; Wang, S.; Xia, G. Large-area rod-coated indium–tin–oxide transparent conductive films for low-cost electronics. *J. Mater. Sci. Mater. Electron.* **2023**, *34*, 2222. [[CrossRef](#)]
125. Dong, L.; Zhu, G.S.; Xu, H.R.; Jiang, X.P.; Zhang, X.Y.; Zhao, Y.Y.; Yan, D.L.; Yuan, L.; Yu, A.B. Preparation of indium tin oxide (ITO) thin film with (400) preferred orientation by sol–gel spin coating method. *J. Mater. Sci. Mater. Electron.* **2019**, *30*, 8047–8054. [[CrossRef](#)]
126. Lei, H.; Wang, M.; Hoshi, Y.; Uchida, T.; Kobayashi, S.; Sawada, Y. Comparative studies on damages to organic layer during the deposition of ITO films by various sputtering methods. *Appl. Surf. Sci.* **2013**, *285*, 389–394. [[CrossRef](#)]
127. Gu, G.; Bulović, V.; Burrows, P.E.; Forrest, S.R.; Thompson, M.E. Transparent organic light emitting devices. *Appl. Phys. Lett.* **1996**, *68*, 2606–2608. [[CrossRef](#)]
128. Burrows, P.E.; Gu, G.; Forrest, S.R.; Vicenzi, E.P.; Zhou, T.X. Semitransparent cathodes for organic light emitting devices. *J. Appl. Phys.* **2000**, *87*, 3080–3085. [[CrossRef](#)]
129. Saikia, D.; Sarma, R. Characterization of organic light-emitting diode using a rubrene interlayer between electrode and hole transport layer. *Bull. Mater. Sci.* **2020**, *43*, 35. [[CrossRef](#)]
130. Meyer, J.; Winkler, T.; Hamwi, S.; Schmale, S.; Johannes, H.; Weimann, T.; Hinze, P.; Kowalsky, W.; Riedl, T. Transparent Inverted Organic Light-Emitting Diodes with a Tungsten Oxide Buffer Layer. *Adv. Mater.* **2008**, *20*, 3839–3843. [[CrossRef](#)]
131. Chen, H.; Qiu, C.; Wong, M.; Kwok, H.S. DC sputtered indium-tin oxide transparent cathode for organic light-emitting diode. *IEEE Electron Device Lett.* **2003**, *24*, 315–317. [[CrossRef](#)]
132. Kanno, H.; Sun, Y.; Forrest, S.R. High-efficiency top-emissive white-light-emitting organic electrophosphorescent devices. *Appl. Phys. Lett.* **2005**, *86*. [[CrossRef](#)]
133. Chauhan, R.N.; Tiwari, N.; Anand, R.S.; Kumar, J. Development of Al-doped ZnO thin film as a transparent cathode and anode for application in transparent organic light-emitting diodes. *RSC Adv.* **2016**, *6*, 86770–86781. [[CrossRef](#)]
134. de Oliveira Xavier Silva, H.; Faraco, T.A.; Maciel, I.O.; Quirino, W.G.; Fragneaud, B.; Pereira, P.G.; Legnani, C. High optoelectronic quality of AZO films grown by RF-magnetron sputtering for organic electronics applications. *Semicond. Sci. Technol.* **2023**, *38*, 065004. [[CrossRef](#)]
135. Lee, J.Y.; Connor, S.T.; Cui, Y.; Peumans, P. Solution-Processed Metal Nanowire Mesh Transparent Electrodes. *Nano Lett.* **2008**, *8*, 689–692. [[CrossRef](#)] [[PubMed](#)]
136. Zeng, X.; Zhang, Q.; Yu, R.; Lu, C. A New Transparent Conductor: Silver Nanowire Film Buried at the Surface of a Transparent Polymer. *Adv. Mater.* **2010**, *22*, 4484–4488. [[CrossRef](#)] [[PubMed](#)]
137. Luka, G.; Krajewski, T.A.; Witkowski, B.S.; Wisz, G.; Virt, I.S.; Guziejewicz, E.; Godlewski, M. Aluminum-doped zinc oxide films grown by atomic layer deposition for transparent electrode applications. *J. Mater. Sci. Mater. Electron.* **2011**, *22*, 1810–1815. [[CrossRef](#)]
138. Bhosle, V.; Prater, J.T.; Yang, F.; Burk, D.; Forrest, S.R.; Narayan, J. Gallium-doped zinc oxide films as transparent electrodes for organic solar cell applications. *J. Appl. Phys.* **2007**, *102*, 023501. [[CrossRef](#)]
139. De, S.; King, P.J.; Lyons, P.E.; Khan, U.; Coleman, J.N. Size Effects and the Problem with Percolation in Nanostructured Transparent Conductors. *ACS Nano* **2010**, *4*, 7064–7072. [[CrossRef](#)] [[PubMed](#)]
140. Formica, N.; Ghosh, D.S.; Chen, T.L.; Eickhoff, C.; Bruder, I.; Pruneri, V. Highly stable Ag–Ni based transparent electrodes on PET substrates for flexible organic solar cells. *Sol. Energy Mater. Sol. Cells* **2012**, *107*, 63–68. [[CrossRef](#)]
141. Yambem, S.D.; Haldar, A.; Liao, K.S.; Dillon, E.P.; Barron, A.R.; Curran, S.A. Optimization of organic solar cells with thin film Au as anode. *Sol. Energy Mater. Sol. Cells* **2011**, *95*, 2424–2430. [[CrossRef](#)]
142. Wu, J.; Agrawal, M.; Becerril, H.A.; Bao, Z.; Liu, Z.; Chen, Y.; Peumans, P. Organic Light-Emitting Diodes on Solution-Processed Graphene Transparent Electrodes. *ACS Nano* **2010**, *4*, 43–48. [[CrossRef](#)] [[PubMed](#)]
143. Yeh, T.H.; Lee, C.C.; Shih, C.J.; Kumar, G.; Biring, S.; Liu, S.W. Vacuum-deposited MoO₃/Ag/WO₃ multilayered electrode for highly efficient transparent and inverted organic light-emitting diodes. *Org. Electron.* **2018**, *59*, 266–271. [[CrossRef](#)]

144. Ohsawa, M.; Hashimoto, N. Flexible transparent electrode of gravure offset printed invisible silver-grid laminated with conductive polymer. *Mater. Res. Express* **2018**, *5*, 085030. [[CrossRef](#)]
145. Cao, W.; Zheng, Y.; Li, Z.; Wrzesniewski, E.; Hammond, W.T.; Xue, J. Flexible organic solar cells using an oxide/metal/oxide trilayer as transparent electrode. *Org. Electron.* **2012**, *13*, 2221–2228. [[CrossRef](#)]
146. Yook, K.S.; Jeon, S.O.; Joo, C.W.; Lee, J.Y. Transparent organic light emitting diodes using a multilayer oxide as a low resistance transparent cathode. *Appl. Phys. Lett.* **2008**, *93*, 013301. [[CrossRef](#)]
147. Kang, M.; Kim, M.; Kim, J.; Guo, L.J. Organic Solar Cells Using Nanoimprinted Transparent Metal Electrodes. *Adv. Mater.* **2008**, *20*, 4408–4413. [[CrossRef](#)]
148. Yu, J.S.; Jung, G.H.; Jo, J.; Kim, J.S.; Kim, J.W.; Kwak, S.W.; Lee, J.L.; Kim, I.; Kim, D. Transparent conductive film with printable embedded patterns for organic solar cells. *Sol. Energy Mater. Sol. Cells* **2013**, *109*, 142–147. [[CrossRef](#)]
149. Oke, J.A.; Jen, T.C. Atomic layer deposition and other thin film deposition techniques: From principles to film properties. *J. Mater. Res. Technol.* **2022**, *21*, 2481–2514. [[CrossRef](#)]
150. Hasselmann, T.; Misimi, B.; Boysen, N.; Zanders, D.; Wree, J.; Rogalla, D.; Haeger, T.; Zimmermann, F.; Brinkmann, K.O.; Schädler, S.; et al. Silver Thin-Film Electrodes Grown by Low-Temperature Plasma-Enhanced Spatial Atomic Layer Deposition at Atmospheric Pressure. *Adv. Mater. Technol.* **2023**, *8*, 2200796. [[CrossRef](#)]
151. Cheylan, S.; Ghosh, D.; Krautz, D.; Chen, T.; Pruneri, V. Organic light-emitting diode with indium-free metallic bilayer as transparent anode. *Org. Electron.* **2011**, *12*, 818–822. [[CrossRef](#)]
152. Hirano, T.; Kawamura, M.; Kiba, T.; Abe, Y.; Kim, K.H.; Hamano, T. Influence of aluminum interlayer on optical properties of very thin silver thin film. *Surf. Coat. Technol.* **2020**, *393*, 125752. [[CrossRef](#)]
153. Wilken, S.; Hoffmann, T.; von Hauff, E.; Borchert, H.; Parisi, J. ITO-free inverted polymer/fullerene solar cells: Interface effects and comparison of different semi-transparent front contacts. *Sol. Energy Mater. Sol. Cells* **2012**, *96*, 141–147. [[CrossRef](#)]
154. Xie, W.; Lau, K.; Lee, C.; Lee, S. Transparent organic light-emitting devices with LiF/Yb:Ag cathode. *Thin Solid Film.* **2007**, *515*, 6975–6977. [[CrossRef](#)]
155. Li, D.; Pan, Y.; Liu, H.; Zhang, Y.; Zheng, Z.; Zhang, F. Study on Ultrathin Silver Film Transparent Electrodes Based on Aluminum Seed Layers with Different Structures. *Nanomaterials* **2022**, *12*, 3540. [[CrossRef](#)] [[PubMed](#)]
156. Hu, B.; Chen, H.; Li, C.; Huang, W.; Ichikawa, M. High-refractive-index capping layer improves top-light-emitting device performance. *Appl. Opt.* **2020**, *59*, 4114. [[CrossRef](#)] [[PubMed](#)]
157. Chae, H.; Park, Y.; Jo, Y.; Jeon, Y.; Lee, H.J.; Yoo, S.; Choi, K.C. Blue Transparent OLEDs with High Stability and Transmittance for Modulating Sleep Disorders. *Adv. Mater. Interfaces* **2023**, *10*, 2202443. [[CrossRef](#)]
158. Lee, I.; Kim, S.; Park, J.Y.; Kim, S.; Cho, H.W.; Ham, J.; Gim, S.; Kim, K.; Hong, K.; Lee, J.L. Symmetrical Emission Transparent Organic Light-Emitting Diodes with Ultrathin Ag Electrodes. *IEEE Photonics J.* **2018**, *10*, 1–10. [[CrossRef](#)]
159. Meiss, J.; Ziehlke, H.; Schubert, S.; Leo, K.; Riede, M. Coevaporated calcium-silver metal alloys as contact for highly transparent organic solar cells. *Energy Sci. Eng.* **2014**, *2*, 77–85. [[CrossRef](#)]
160. Ji, C.; Liu, D.; Zhang, C.; Guo, L.J. Ultrathin-metal-film-based transparent electrodes with relative transmittance surpassing 100%. *Nat. Commun.* **2020**, *11*, 3367. [[CrossRef](#)] [[PubMed](#)]
161. Song, M.G.; Kim, K.S.; Yang, H.I.; Kim, S.K.; Kim, J.H.; Han, C.W.; Choi, H.C.; Pode, R.; Kwon, J.H. Highly reliable and transparent Al doped Ag cathode fabricated using thermal evaporation for transparent OLED applications. *Org. Electron.* **2020**, *76*, 105418. [[CrossRef](#)]
162. MacLeod, H.A.; Macleod, H.A. *Thin-Film Optical Filters*; CRC Press: Boca Raton, FL, USA, 2010. [[CrossRef](#)]
163. Shinar, J.; Shinar, R. *An Overview of Organic Light-Emitting Diodes and their Applications*; Elsevier: Amsterdam, The Netherland, 2011; pp. 73–107. [[CrossRef](#)]
164. Tian, B.; Williams, G.; Ban, D.; Aziz, H. Transparent organic light-emitting devices using a MoO₃/Ag/MoO₃ cathode. *J. Appl. Phys.* **2011**, *110*, 104507. [[CrossRef](#)]
165. Cattin, L.; Morsli, M.; Dahou, F.; Abe, S.Y.; Khelil, A.; Bernède, J. Investigation of low resistance transparent MoO₃/Ag/MoO₃ multilayer and application as anode in organic solar cells. *Thin Solid Films* **2010**, *518*, 4560–4563. [[CrossRef](#)]
166. Wrzesniewski, E. Transparent oxide/metal/oxide trilayer electrode for use in top-emitting organic light-emitting diodes. *J. Photonics Energy* **2011**, *1*, 011023. [[CrossRef](#)]
167. Choi, D.K.; Kim, D.H.; Lee, C.M.; Hafeez, H.; Sarker, S.; Yang, J.S.; Chae, H.J.; Jeong, G.W.; Choi, D.H.; Kim, T.W.; et al. Highly efficient, heat dissipating, stretchable organic light-emitting diodes based on a MoO₃/Au/MoO₃ electrode with encapsulation. *Nat. Commun.* **2021**, *12*, 2864. [[CrossRef](#)] [[PubMed](#)]
168. Cho, H.; Yun, C.; Park, J.W.; Yoo, S. Highly flexible organic light-emitting diodes based on ZnS/Ag/WO₃ multilayer transparent electrodes. *Org. Electron.* **2009**, *10*, 1163–1169. [[CrossRef](#)]
169. Han, Y.C.; Lim, M.S.; Park, J.H.; Choi, K.C. ITO-free flexible organic light-emitting diode using ZnS/Ag/MoO₃ anode incorporating a quasi-perfect Ag thin film. *Org. Electron.* **2013**, *14*, 3437–3443. [[CrossRef](#)]
170. Liu, X. The design of ZnS/Ag/ZnS transparent conductive multilayer films. *Thin Solid Films* **2003**, *441*, 200–206. [[CrossRef](#)]
171. Sharma, V.; Kumar, P.; Kumar, A.; Surbhi; Asokan, K.; Sachdev, K. High-performance radiation stable ZnO/Ag/ZnO multilayer transparent conductive electrode. *Sol. Energy Mater. Sol. Cells* **2017**, *169*, 122–131. [[CrossRef](#)]
172. Hajj, A.E.; Lucas, B.; Chakaroun, M.; Antony, R.; Ratier, B.; Aldissi, M. Optimization of ZnO/Ag/ZnO multilayer electrodes obtained by Ion Beam Sputtering for optoelectronic devices. *Thin Solid Film.* **2012**, *520*, 4666–4668. [[CrossRef](#)]

173. Kim, J.H.; Lee, J.H.; Kim, S.W.; Yoo, Y.Z.; Seong, T.Y. Highly flexible ZnO/Ag/ZnO conducting electrode for organic photonic devices. *Ceram. Int.* **2015**, *41*, 7146–7150. [[CrossRef](#)]
174. Kang, S.K.; Kang, D.Y.; Park, J.W.; Son, K.R.; Kim, T.G. Work function-tunable ZnO/Ag/ZnO film as an effective hole injection electrode prepared via nickel doping for thermally activated delayed fluorescence-based flexible blue organic light-emitting diodes. *Appl. Surf. Sci.* **2021**, *538*, 148202. [[CrossRef](#)]
175. Girtan, M. Comparison of ITO/metal/ITO and ZnO/metal/ZnO characteristics as transparent electrodes for third generation solar cells. *Sol. Energy Mater. Sol. Cells* **2012**, *100*, 153–161. [[CrossRef](#)]
176. Yu, S.; Li, L.; Lyu, X.; Zhang, W. Preparation and investigation of nano-thick FTO/Ag/FTO multilayer transparent electrodes with high figure of merit. *Sci. Rep.* **2016**, *6*, 20399. [[CrossRef](#)] [[PubMed](#)]
177. Park, S.H.; Lee, S.J.; Lee, J.H.; Kal, J.; Hahn, J.; Kim, H.K. Large area roll-to-roll sputtering of transparent ITO/Ag/ITO cathodes for flexible inverted organic solar cell modules. *Org. Electron.* **2016**, *30*, 112–121. [[CrossRef](#)]
178. Lee, D.; Song, M.S.; Seo, Y.H.; Lee, W.W.; Kim, Y.W.; Park, M.; Shin, Y.J.; Kwon, S.J.; Jeon, Y.; Cho, E.S. Highly Transparent Red Organic Light-Emitting Diodes with AZO/Ag/AZO Multilayer Electrode. *Micromachines* **2024**, *15*, 146. [[CrossRef](#)] [[PubMed](#)]
179. Chen, X.; Wu, D.; Wang, J.; Zhou, Y.; Zhang, Z.; Li, C.; Zhang, J.; Chen, P.; Duan, Y. A highly transparent laminated composite cathode for organic light-emitting diodes. *Appl. Phys. Lett.* **2021**, *119*, 073301. [[CrossRef](#)]
180. Park, S.; Lim, J.T.; Jin, W.Y.; Lee, H.; Kwon, B.H.; Cho, N.S.; Han, J.H.; Kang, J.W.; Yoo, S.; Lee, J.I. Efficient Large-Area Transparent OLEDs Based on a Laminated Top Electrode with an Embedded Auxiliary Mesh. *ACS Photonics* **2017**, *4*, 1114–1122. [[CrossRef](#)]
181. Bae, H.W.; Kim, S.K.; Lee, S.; Song, M.; Lampande, R.; Kwon, J.H. Thermally Evaporated Organic/Ag/Organic Multilayer Transparent Conducting Electrode for Flexible Organic Light-Emitting Diodes. *Adv. Electron. Mater.* **2019**, *5*, 1900620. [[CrossRef](#)]
182. Kim, S.K.; Lampande, R.; Kwon, J.H. Electro-optically Efficient and Thermally Stable Multilayer Semitransparent Pristine Ag Cathode Structure for Top-Emission Organic Light-Emitting Diodes. *ACS Photonics* **2019**, *6*, 2957–2965. [[CrossRef](#)]
183. Xu, M.; Jiao, S.; Liu, M.; Liu, Y.; Cao, W.; Wu, Y.C.; Zhou, H. Highly Efficiency Top-Emitting Organic Light-Emitting Diode with Double Capping Layers. In Proceedings of the 2019 IEEE International Conference on Electron Devices and Solid-State Circuits (EDSSC), Xi'an, China, 12–14 June 2019; pp. 1–2. [[CrossRef](#)]
184. Joo, C.W.; Shin, J.W.; Moon, J.; Huh, J.W.; Cho, D.H.; Lee, J.; Park, S.K.; Cho, N.S.; Han, J.H.; Chu, H.Y.; et al. Highly efficient white transparent organic light emitting diodes with nano-structured substrate. *Org. Electron.* **2016**, *29*, 72–78. [[CrossRef](#)]
185. Mauro, A.D.G.D.; Lepera, E.; Bruno, A.; Fasolino, T.; Maglione, M.; Nenna, G.; Minarini, C. Light extraction in organic light-emitting diode using PDMS/TiO₂ scattering substrates. In Proceedings of the 2014 Fotonica AEIT Italian Conference on Photonics Technologies, Naples, Italy, 12–14 May 2014; pp. 1–4. [[CrossRef](#)]
186. Kim, D.Y.; Choi, C.S.; Kim, J.Y.; Kim, D.H.; Choi, K.C. Phosphorescent transparent organic light-emitting diodes with enhanced outcoupling efficiency: Reduction of surface plasmon losses. *Org. Electron.* **2014**, *15*, 1222–1228. [[CrossRef](#)]
187. Huh, J.W.; Shin, J.W.; Cho, D.H.; Moon, J.; Joo, C.W.; Park, S.K.; Hwang, J.; Cho, N.S.; Lee, J.; Han, J.H.; et al. A randomly nano-structured scattering layer for transparent organic light emitting diodes. *Nanoscale* **2014**, *6*, 10727–10733. [[CrossRef](#)] [[PubMed](#)]
188. Ran, G.Z.; Zhao, W.Q.; Ma, G.L.; Dai, L.; Qin, G.G. Role of the dielectric capping layer in enhancement of light outcoupling for semitransparent metal-cathode organic light-emitting devices. *J. Opt. A Pure Appl. Opt.* **2006**, *8*, 733–736. [[CrossRef](#)]
189. Lee, J.W.; Lee, J.; Chu, H.Y.; Lee, J.I. Controlling the optical efficiency of the transparent organic light-emitting diode using capping layers. *J. Inf. Disp.* **2013**, *14*, 57–60. [[CrossRef](#)]
190. Tan, G.; Lee, J.H.; Lin, S.C.; Zhu, R.; Choi, S.H.; Wu, S.T. Analysis and optimization on the angular color shift of RGB OLED displays. *Opt. Express* **2017**, *25*, 33629. [[CrossRef](#)]
191. Hong, K.; Lee, J.L. Review paper: Recent developments in light extraction technologies of organic light emitting diodes. *Electron. Mater. Lett.* **2011**, *7*, 77–91. [[CrossRef](#)]
192. Park, C.H.; Kim, J.G.; Jung, S.G.; Lee, D.J.; Park, Y.W.; Ju, B.K. Optical characteristics of refractive-index-matching diffusion layer in organic light-emitting diodes. *Sci. Rep.* **2019**, *9*, 8690. [[CrossRef](#)] [[PubMed](#)]
193. Mohamed, S.H.; El-Hagary, M.; Emam-Ismail, M. Thickness and annealing effects on the optoelectronic properties of ZnS films. *J. Phys. D Appl. Phys.* **2010**, *43*, 075401. [[CrossRef](#)]
194. Subrahmanyam, A.; Karuppasamy, A. Optical and electrochromic properties of oxygen sputtered tungsten oxide (WO₃) thin films. *Sol. Energy Mater. Sol. Cells* **2007**, *91*, 266–274. [[CrossRef](#)]
195. Kwon, B.H.; Lee, H.; Kim, M.; Joo, C.W.; Cho, H.; Lim, J.T.; Jung, Y.S. A Systematic Study of the Interactions in the Top Electrode/Capping Layer/Thin Film Encapsulation of Transparent OLEDs. *J. Ind. Eng. Chem.* **2021**, *93*, 237–244. [[CrossRef](#)]
196. Haacke, G. New figure of merit for transparent conductors. *J. Appl. Phys.* **1976**, *47*, 4086–4089. [[CrossRef](#)]
197. Anand, A.; Islam, M.M.; Meitzner, R.; Schubert, U.S.; Hoppe, H. Introduction of a Novel Figure of Merit for the Assessment of Transparent Conductive Electrodes in Photovoltaics: Exact and Approximate Form. *Adv. Energy Mater.* **2021**, *11*, 2100875. [[CrossRef](#)]
198. Ji, W.; Zhao, J.; Sun, Z.; Xie, W. High-color-rendering flexible top-emitting warm-white organic light emitting diode with a transparent multilayer cathode. *Org. Electron.* **2011**, *12*, 1137–1141. [[CrossRef](#)]
199. Lu, H.W.; Huang, C.W.; Kao, P.C.; Chu, S.Y. ITO-free organic light-emitting diodes with MoO₃/Al/MoO₃ as semitransparent anode fabricated using thermal deposition method. *Appl. Surf. Sci.* **2015**, *347*, 116–121. [[CrossRef](#)]

200. Ryu, S.Y.; Noh, J.H.; Hwang, B.H.; Kim, C.S.; Jo, S.J.; Kim, J.T.; Hwang, H.S.; Baik, H.K.; Jeong, H.S.; Lee, C.H.; et al. Transparent organic light-emitting diodes consisting of a metal oxide multilayer cathode. *Appl. Phys. Lett.* **2008**, *92*, 023306. [[CrossRef](#)]
201. Guillén, C.; Herrero, J. ITO/metal/ITO multilayer structures based on Ag and Cu metal films for high-performance transparent electrodes. *Sol. Energy Mater. Sol. Cells* **2008**, *92*, 938–941. [[CrossRef](#)]
202. Park, J.W.; Shin, D.C.; Park, S.H. Large-area OLED lightings and their applications. *Semicond. Sci. Technol.* **2011**, *26*, 034002. [[CrossRef](#)]
203. Ye, T.; Jun, L.; Kun, L.; Hu, W.; Ping, C.; Duan, Y.-H.; Zheng, C.; Liu, Y.-F.; Wang, H.-R.; Yu, D. Inkjet-printed Ag grid combined with Ag nanowires to form a transparent hybrid electrode for organic electronics. *Org. Electron.* **2017**, *41*, 179–185. [[CrossRef](#)]
204. Yu, J.H.; Cho, K.H.; Kang, K.T.; Cho, Y.I.; Lee, C.S.; Lee, S.H. 64-2: Fabrication of Auxiliary Electrodes using Ag Inkjet Printing for OLED Lighting. *SID Symp. Dig. Tech. Pap.* **2018**, *49*, 843–846. [[CrossRef](#)]
205. Sim, S.M.; Yu, J.H.; Cho, K.H.; Lee, S.H. Self-aligned bilayer inkjet printing process for reducing shadow area by auxiliary electrodes in OLED lighting. *Org. Electron.* **2022**, *111*, 106672. [[CrossRef](#)]
206. Neyts, K.; Marescaux, M.; Nieto, A.U.; Elschner, A.; Lövenich, W.; Fehse, K.; Huang, Q.; Walzer, K.; Leo, K. Inhomogeneous luminance in organic light emitting diodes related to electrode resistivity. *J. Appl. Phys.* **2006**, *100*, 114513. [[CrossRef](#)]
207. Neyts, K.; Real, A.; Marescaux, M.; Mladenovski, S.; Beeckman, J. Conductor grid optimization for luminance loss reduction in organic light emitting diodes. *J. Appl. Phys.* **2008**, *103*, 093113. [[CrossRef](#)]
208. Ghosh, D.S.; Chen, T.L.; Pruneri, V. High figure-of-merit ultrathin metal transparent electrodes incorporating a conductive grid. *Appl. Phys. Lett.* **2010**, *96*, 041109. [[CrossRef](#)]
209. Burwell, G.; Burr ridge, N.; Sandberg, O.J.; Bond, E.; Li, W.; Meredith, P.; Armin, A. Metal Grid Structures for Enhancing the Stability and Performance of Solution-Processed Organic Light-Emitting Diodes. *Adv. Electron. Mater.* **2020**, *6*, 2000732. [[CrossRef](#)]
210. Fakharan, Z.; Dabirian, A. Metal grid technologies for flexible transparent conductors in large-area optoelectronics. *Curr. Appl. Phys.* **2021**, *31*, 105–121. [[CrossRef](#)]
211. Morales-Masis, M.; Dazou, F.; Jeangros, Q.; Dabirian, A.; Lifka, H.; Gierth, R.; Ruske, M.; Moet, D.; Hessler-Wyser, A.; Ballif, C. An Indium-Free Anode for Large-Area Flexible OLEDs: Defect-Free Transparent Conductive Zinc Tin Oxide. *Adv. Funct. Mater.* **2016**, *26*, 384–392. [[CrossRef](#)]
212. Urich, C.; Weiß, A.; Pfeiffer, M. Roll-to-roll production of organic solar cells. In Proceedings of the Organic, Hybrid, and Perovskite Photovoltaics XVIII, San Diego, CA, USA, 6–10 August 2017; Kafafi, Z.H., Lane, P.A., Lee, K., Eds.; International Society for Optics and Photonics, SPIE: Bellingham, WA, USA, 2017; Volume 10363, p. 103630F. [[CrossRef](#)]
213. Seetharaman, M.; Pillai, G.; Rana, R.; Awasthi, A.; Krishnamanohara, Balakrishnan, M.; Katiyar, M. Challenges and Approaches towards Defect Free Large Area Organic Light Emitting Diode Fabrication. In Proceedings of the 2022 IEEE International Conference on Emerging Electronics (ICEE), Bangalore, India, 11–14 December 2022; pp. 1–4. [[CrossRef](#)]
214. Ding, Z.; Kim, H.; Lee, D.; Stickel, S.; Boroson, M.; Hamer, J.; Giebink, N.C. The nature of catastrophic OLED lighting panel failure. *J. Appl. Phys.* **2019**, *125*, 055501. [[CrossRef](#)]
215. Solanki, A.; Awasthi, A.; Unni, K.N.N.; Deepak. An efficient and facile method to develop defect-free OLED displays. *Semicond. Sci. Technol.* **2021**, *36*, 065005. [[CrossRef](#)]
216. Riahi, M.; Yoshida, K.; Hafeez, H.; Samuel, I.D.W. Improving the Uniformity of Top Emitting Organic Light Emitting Diodes Using a Hybrid Electrode Structure. *Adv. Electron. Mater.* **2024**, *10*, 2300675. [[CrossRef](#)]

Disclaimer/Publisher’s Note: The statements, opinions and data contained in all publications are solely those of the individual author(s) and contributor(s) and not of MDPI and/or the editor(s). MDPI and/or the editor(s) disclaim responsibility for any injury to people or property resulting from any ideas, methods, instructions or products referred to in the content.